

**EFFECT OF LESSER TUBEROSITY OSTEOTOMY SIZE AND REPAIR CONSTRUCT
DURING TOTAL SHOULDER ARTHROPLASTY**

by

Brandon T. Brown

B.S. in Bioengineering, Syracuse University, 2009

Submitted to the Graduate Faculty of
Swanson School of Engineering in partial fulfillment
of the requirements for the degree of
Master of Science in Mechanical Engineering

University of Pittsburgh

2013

UNIVERSITY OF PITTSBURGH
SWANSON SCHOOL OF ENGINEERING

This thesis was presented

by

Brandon T. Brown

It was defended on

April 1st, 2013

and approved by

Jeffrey Vipperman, PhD, Associate Professor, Department of
Mechanical Engineering and Materials Science

Xudong Zhang, PhD, Associate Professor, Department of
Mechanical Engineering and Materials Science

Patrick Smolinski, PhD, Associate Professor, Department of
Mechanical Engineering and Materials Science

Thesis Advisor: Mark Carl Miller, PhD, Associate Research Professor, Department of
Mechanical Engineering and Materials Science

Copyright © by Brandon T. Brown

2013

EFFECT OF LESSER TUBEROSITY OSTEOTOMY SIZE AND REPAIR CONSTRUCT DURING TOTAL SHOULDER ARTHROPLASTY

Brandon T. Brown, M.S.

University of Pittsburgh, 2013

Background. Lesser tuberosity osteotomy has been shown to decrease post-operative subscapularis dysfunction. The purpose of this study was to determine the effect of osteotomy thickness and suture configuration on repair integrity.

Methods. One side of twelve matched-pair cadaveric shoulders was randomly assigned either a thick osteotomy (100% lesser tuberosity height) or a thin (50% height) osteotomy. Both sides of the matched-pairs were given the same repair, either 1) compression-sutures or 2) compression-sutures plus one tension-suture. This created four groups of six paired specimens. CT imaging measured tuberosity dimensions pre- and post-osteotomy to validate fragment height and area. The repairs were loaded cyclically and then loaded to failure. A video system measured fragment displacement. Percent area of osteotomy contact was calculated from the CT and displacement data.

Results. The average initial displacement was less in the thin osteotomy groups ($p=0.011$). Adding a tension-suture negated this difference. A significant number of thin compared to thick repair sites remained intact during load to failure ($p=0.001$). No difference occurred due to maximal load between the repair groups ($p=0.40$) and construct stiffness was greater when a tension-suture was used ($p=0.032$). Percent area of osteotomy contact revealed no differences between the osteotomy ($p=0.431$) and repair ($p=0.25$) groups.

Conclusion. The study showed that thin osteotomies displaced less than thick osteotomies. Adding a tension band improved construct stability and eliminated some failure modes. The ideal repair was a thin wafer with both tension and compression sutures. This construct had smaller total displacement, a reasonable osteotomy percent contact area, and acceptable maximum load.

TABLE OF CONTENTS

PREFACE.....	XI
1.0 INTRODUCTION.....	1
1.1 MOTIVATION	1
1.2 GOALS	2
2.0 BACKGROUND	3
2.1 ANATOMIC DEFINITIONS	3
2.2 THE SHOULDER	4
2.3 SHOULDER MECHANICS AND THE SUBSCAPULARIS.....	6
2.4 TOTAL SHOULDER ARTHROPLASTY.....	8
2.5 SUBSCAPULARIS REPAIR.....	9
2.5.1 Technique Comparisons.....	10
2.5.2 Lesser Tuberosity Osteotomy	11
2.6 PREVIOUS WORK ON MECHANICAL TESTING OF LESSER TUBEROSITY OSTEOTOMIES	13
2.7 IMAGING	18
2.7.1 Bone Mineral Density Estimations.....	19
3.0 METHODS	21
3.1 PROJECT OVERVIEW	21

3.2	STUDY DESIGN	22
3.3	CADAVERIC TISSUE.....	23
3.4	OSTEOTOMY TECHNIQUE, BONE MINERAL DENSITY AND AREA	24
3.5	SURGICAL REPAIR TECHNIQUE	26
3.6	BIOMECHANICAL TESTING.....	27
3.6.1	Material Testing System	28
3.6.2	Displacement Measurement.....	30
3.6.3	Testing.....	33
3.7	STATISTICS.....	39
4.0	RESULTS	40
4.1	SPECIMENS	40
4.2	OSTEOTOMIES.....	40
4.3	DISPLACEMENT DATA.....	41
4.4	STRUCTURAL PROPERTIES	43
4.5	FAILURE MODES.....	44
5.0	DISCUSSION	46
6.0	CONCLUSIONS AND FUTURE WORK	55
6.1	CONCLUSION	55
6.2	FUTURE WORK.....	55
APPENDIX A		57
DATA ACQUISITION MATLAB CODE		57
APPENDIX B		59
DISPLACEMENT COMPUTATIONS MATLAB CODE.....		59

APPENDIX C	74
OSTEOTOMY CONTACT AREA CODE	74
APPENDIX D	87
OSTEOTOMY EDGE TRACKING TECHNIQUE	87
BIBLIOGRAPHY	92

LIST OF TABLES

Table 1: Data from the experiment.	41
Table 2: Comparisons from other publications.....	51

LIST OF FIGURES

Figure 1: Schematic of an anterior view of the shoulder joint.....	5
Figure 2: A schematic illustrating the two common repair techniques.	13
Figure 3: A schematic showing the partially nested experimental design.....	23
Figure 4: The figure shows the thick and thin osteotomies of specimen number 3025.....	24
Figure 5: Diagram and photos illustrating the two repair types.....	27
Figure 6: Image of the material testing system used for this experiment	29
Figure 7: Image of the calibration frame used for this experiment.....	33
Figure 8: Photograph of the mechanical testing setup	35
Figure 9: Schematic of cyclic testing protocol and subsequent calculations.....	36
Figure 10: Load to failure output of a typical specimen with subsequent calculations.....	37
Figure 11: Diagram depicting the calculation for osteotomy contact area after cyclic testing.....	38
Figure 12: Results of the displacement and mechanical data for all tests groups.....	43
Figure 13: Frequency diagram for the failure modes observed during the load to failure test.....	45

PREFACE

This work would not have been possible without the help of key individuals and partial funding by Zimmer Inc. I would like to thank David Weir for his assistance in organizing, executing and analyzing aspects of this experiment I would also like to express my gratitude towards Zimmer Inc. for supplying part of the funding necessary to complete this project. I would also like to thank the individuals in the Allegheny Biomechanics Laboratory for their assistance in performing the tasks related to this project. Last, but not least, I would like to thank Dr. Christopher Schmidt for his contributions to the research and his support of my goal to pursue higher education.

1.0 INTRODUCTION

1.1 MOTIVATION

Anatomic replacement of the shoulder joint requires alteration and repair of the subscapularis tendon in order to access the joint. As a muscle of the rotator cuff, the subscapularis muscle is a key stabilizer of the shoulder joint. It is critical to have a functional subscapularis muscle for the success of a total shoulder replacement (TSA). Osteotomy of the lesser tuberosity is a popular method of repair that relies on the more predictable healing properties of bone instead of less certain healing properties of the tendon, seen in other techniques. Lesser tuberosity osteotomy is a reliable technique for fixation of the subscapularis tendon onto the humerus to achieve a functional subscapularis muscle post operation, however, within this repair lie several variables that can affect the outcome that are not well understood.

The osteotomy of the lesser tuberosity involves removing a portion of the tuberosity from the humerus. The optimal bone wafer size to remove is not well known; too little will not promote healing and too large will be detrimental to the structure of the humerus risking failure of the shoulder replacement. Furthermore, fixation of the lesser tuberosity fragment onto the humerus is an area of debate. Two prevalent and distinct techniques have been used with success clinically.^{23, 32, 34, 38} Each technique has been separately tested and clinically evaluated, however there has been no investigation into the effects of combining these techniques in an effort to

improve the mechanical stability and success rate of the repairs. Currently an individual must be immobilized for six weeks because of weaknesses in the lesser tuberosity osteotomy; allowing individuals who receive a TSA to return to activity sooner might increase the overall success of this procedure because earlier activity would inhibit adhesions and promote healing.

In an effort to decrease the weaknesses observed in the current techniques it has been hypothesized that combination of suture techniques with optimal osteotomy thickness could produce a better repair. Mechanical analysis of the osteotomy repairs *in vitro* will allow quantification of the suture and osteotomy thickness effects. Measurement of the load capacity of these repairs and the associated displacement at the repair site will be the main means of evaluation of the repairs. This information will be used to establish criteria for optimal osteotomy thickness and determine effects of repair configuration.

1.2 GOALS

The purpose of this study was to determine the effect of osteotomy thickness on the mechanical behavior of two repair constructs. The two repair constructs differed in suture configuration: a compression style repair in which suture wraps around the humeral stem and a tension style repair where a suture is added to the compression repair and secured using a lateral buttress plate. The hypotheses were i) thick osteotomy wafers will fail at higher maximum loads than thin wafers, ii) tension style repairs will fail at higher maximal loads and demonstrate less medial displacement with cyclical loading and, iii) differences in repair techniques will be more pronounced in the thin osteotomy group than the thick group because there should be more structural support from the bone fragment.

2.0 BACKGROUND

2.1 ANATOMIC DEFINITIONS

The human body is a complex object where numerous rotations and positions of all the limbs can occur. When discussing anatomical locations and features it helps to have a standard frame of reference known as the anatomical position. In this position, the body stands with the arms at the side and the palms facing towards the front. All of the terms defined hereafter apply to this anatomical position. Reference planes provide divisions of the body. The horizontal plane divides the body axially. This plane separates the legs from the upper body if it placed at the hips. The coronal plane divides the body vertically in a manner that separates the front from the back. This plane could be thought of as connecting the shoulders and extending down to the feet. The third orthogonal plane is known as the sagittal plane; this plane divides the body in half vertically separating left from right.

Other terms further classify and organize the body. Anterior and posterior describe the front and back side of the body, respectively. Bisection of the body down the middle in the sagittal plane would be called the midline. Lateral is away from this midline and medial is towards this midline. Superior and inferior refer to location up and down parallel to the horizontal plane. The final common necessary terms are proximal and distal, used to describe the proximity to the center of the body. Distal is further down than proximal; for example, the

elbow is distal to the shoulder but proximal to the hand. These terms are used frequently throughout this manuscript to describe aspects of the background and experimental methodology.

2.2 THE SHOULDER

The shoulder is composed of multiple joints that allow a large range of motion. The subscapularis tendon and muscle are parts of this shoulder joint complex. Three bones comprise the shoulder joint: the humerus, scapula and clavicle. These bones form the glenohumeral, acromioclavicular and sternoclavicular joints seen in Figure 1. There is significant ligamentous support at all joints as well as a large ligament between the acromion and coracoid process of the scapula known as the coracoacromial ligament.³⁰ There are over 18 different muscles that support and move the shoulder; the subscapularis muscle is one of them.^{7, 16} The humerus has a large convex head at its proximal end which fits into the concave glenoid cavity of the scapula which is roughly 1/3 the size of the humeral head, Figure 1. In the normal shoulder, this arrangement allows a large range of motion for the humerus. The glenoid is part of in the scapula, which can also move, thus producing an even larger range of motion. This large range of motion produces a fundamentally unstable system which is countered in the body by ligamentous and muscular support. To keep the motion as dynamic as possible, the capsule of the shoulder joint is far more relaxed than any other joint in the body, which requires muscular and ligamentous forces to keep the joint from stable. Key structures in the stability of this system are the muscles of the rotator cuff: the infraspinatus, supraspinatus, teres minor, and subscapularis. Figure 1 shows the subscapularis muscle and its location within the shoulder. The muscle originates on the anterior medial side of the scapula in the subscapular fossa and attaches

to the lesser tuberosity of the humerus, Figure 1. The subscapularis muscle is innervated by the superior and inferior subscapularis nerves and is thus divided into three functioning parts: the superior, middle and inferior sections. This muscle is the largest and most powerful in the rotator cuff group and is crucial for glenohumeral joint stability.¹⁶

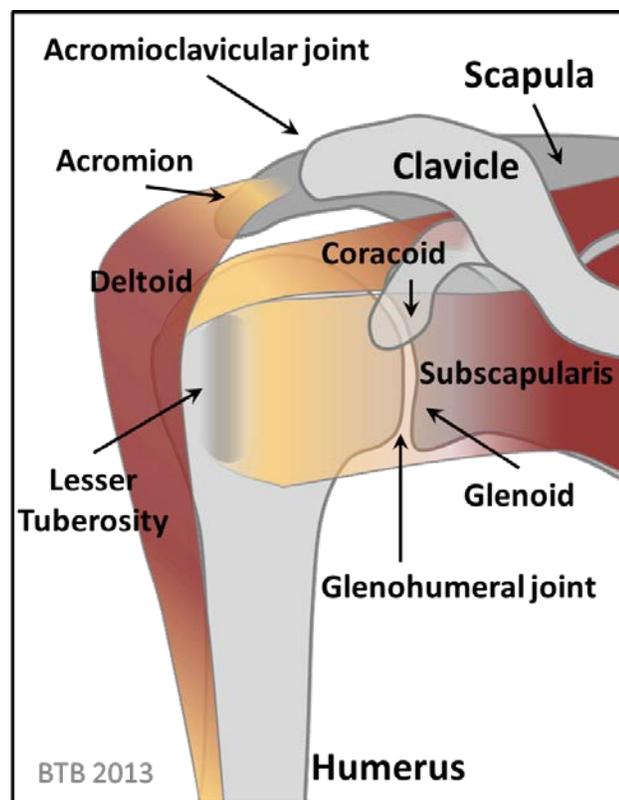


Figure 1: Schematic of an anterior view of the shoulder joint.

2.3 SHOULDER MECHANICS AND THE SUBSCAPULARIS

The shoulder has a large range of motion; the joint is defined as a loose ball and socket joint. Terms associate with shoulder motion are adduction–abduction; flexion–extension, and internal–external rotation. The shoulder performs abduction and adduction in the coronal plane; abduction occurs when the arm moves away from the midline, adduction moves closer to the midline. In the sagittal plane, the shoulder flexes and extends; flexion occurs when the arm is raised, anteriorly, in front of the body; extension occurs when the arm is raised posteriorly. The third direction of motion is internal and external rotation, which is rotation about the long axis of the humerus: internal rotation brings the hand closer to the midline of the body when the forearm is flexed at 90 degrees starting from the anatomic position; external rotation moves the hand away from the body when starting at the same initial position. The subscapularis muscle always effects internal rotation and adduction, and can extend the shoulder in some postures. Often clinical evaluation of the subscapularis muscle involves a person attempting to tuck a shirt in behind their back.²¹ The subscapularis also acts as important stabilizer of the glenohumeral joint by preventing anterior translation of the humeral head on the glenoid cavity. Not only does the passive tension of the muscle prevent anterior translation of the humerus, but muscle activity produces further tension, compressing the convex head of the humerus into the concave cavity of the glenoid, stabilizing the joint.

Kinematic studies have highlighted the importance of the subscapularis muscle in joint stability; in fact, the greater the abduction in the shoulder, the greater the compressive line of action becomes for the subscapularis.⁷ Ackland et al. demonstrated that the moments produced by the subscapularis promote compression of the humerus into the glenoid cavity.⁸ Furthermore when analyzing the three compartments of the subscapularis, Ackland et al. found that with

shoulder abduction, the inferior portion of the subscapularis had a higher moment arm and when the arm is adducted into the body, the superior and middle portions had higher moment arms.⁸ A separate analysis involving positron emission tomography (PET), which mapped muscle activity, showed that the subscapularis co-contracted with the deltoid to stabilize the joint during abduction.³⁶ Study of abnormal or injured subscapularis function has promoted further understanding of the importance of the subscapularis in normal shoulder function. Kedgley et al. established that the plane of abduction moved posteriorly and became more abnormal throughout abduction with increasing subscapularis tendon tear size.³ Subscapularis transection doubled translation of the humerus in the glenoid. Similarly, Marquart et al. found that removal of the subscapularis tendon removal doubled the laxity of the joint.⁴ Further investigation demonstrated that when the subscapularis was deficient, the ability to abduct decreased by 16% due to destabilization.²⁸ These results highlight requirements for subscapularis repair and show that the subscapularis is a key factor in stabilizing the joint in the anterior and inferior directions.

The final piece of information needed to ensure adequate subscapularis repair is the normal kinetic environment of the shoulder; determination of the forces at the shoulder involves mechanical testing of the uninjured subscapularis. Numerous studies quantified the average and peak forces in the subscapularis during shoulder movement. The highest rotator cuff muscle force during maximal internal rotation originates in the subscapularis.³⁷ Invasive studies have been performed using arthroscopically implantable force probes directly into the subscapularis *in vivo* in an attempt to quantify the muscle force. Two studies have been performed and estimate the subscapularis can generate a force of 250 N during maximal internal rotation.^{6, 31} The combination of kinematic data and force data allows the design of subscapularis repairs to

consider the normal contractile force and the normal shoulder range of motion. Successful subscapularis repairs will contribute to successful total shoulder replacement (arthroplasty).

2.4 TOTAL SHOULDER ARTHROPLASTY

Total shoulder arthroplasty (TSA) is the act of replacing the humeral head and the glenoid with articulating artificial surfaces. Indications for TSA are osteoarthritis, rheumatoid arthritis, post-traumatic arthritis, rotator cuff insufficiency, avascular necrosis, humeral fracture, and failed previous shoulder replacement surgery.¹ The procedure seeks to alleviate pain while restoring normal function to the shoulder. In 2011, a study found about 53,000 people per year receive a total shoulder arthroplasty; this compares to 900,000 knee and hip replacements, separately, per year.¹ Improved operative techniques, devices and success rates have increased the number of shoulder replacements even two years later. Although the current methods of TSA produce adequate outcomes, many repairs do not replicate normal physiologic function. The original purpose of TSA was to improve mobility of severely disabled individuals, often the elderly, with expectations of relatively short-term device survival. However, with device improvement and longer life expectancies, there is demand for greater device survival and more overall function; thus techniques and devices need improvement to meet this demand.

TSA accesses the deepest part of the joint itself, because the head of the humerus is replaced. Much like a knee or hip replacement, a surgeon must temporarily move or completely cut structures in order to implant the replacement.¹ Total shoulder arthroplasty often alters the subscapularis tendon during the procedure. Function of the subscapularis with the implanted device and repair techniques are key factors in success of the TSA.^{5, 13, 21, 24, 25, 27} TSA removes

the head of the humerus and replaces it with a humeral component, the shaft of which fits into the humeral canal. The glenoid is reamed for placement of the glenoid component; the surfaces are then matched and the subscapularis tendon is repaired. Replacement of the glenohumeral joint removes the stability of the joint capsule and thus the replacement relies heavily on muscular support.^{10, 24} Subscapularis tendon rupture or avulsion after TSA often leads to pain, weakness, decreased active motion, anterior instability, reduced functional outcome scores, and even premature glenoid loosening; dysfunction can result in loss of terminal internal rotation strength.^{21, 25-27, 38, 40} Repair of the subscapularis to produce function similar to the native state is crucial for the success of the TSA and the improved methods to achieve this result are currently under investigation.

2.5 SUBSCAPULARIS REPAIR

A review article prepared by DeFranco et al. in 2010 describes the subscapularis muscle and its management during TSA. There are four main ways to repair the subscapularis tendon: i) tendon-bone (Subscapularis Peel), ii) Z-Plasty (a variation of tendon to tendon), iii) tendon-tendon (Tenotomy), and iv) bone-bone (Osteotomy) repairs.²⁴ i) The Subscapularis Peel technique elevates the subscapularis tendon at the insertion site on the lesser tuberosity and involves subsequent bone tunnels for fixation of the tendon with nonabsorbable sutures. ii) The Z plasty technique involves cutting the tendon slightly before its insertion, then filleting the longer part of the tendon and suturing it to the insertion site to lengthen the repair. iii) The tenotomy involves cutting the tendon at the midpoint between the periosteal insertion and musculotendinous junction. The fibers are then sutured together in the hopes that the tissue will

revascularize and repair itself with the proper orientation. iv) The osteotomy involves removal of the lesser tuberosity with the tendon insertion so that it can be secured back into place once the procedure is complete. This is typically performed using transosseous sutures or a titanium plate, to aid in mechanical stability during the initial post-operative period. The tenotomy and osteotomy are the most popular and successful techniques in TSA²⁴. The inability to achieve a repair with normal or near normal structural and biomechanical strength is a primary reason for unsatisfactory function and failure at the subscapularis repair site.²⁴

2.5.1 Technique Comparisons

Each technique has its disadvantages. Subscapularis peel is the most difficult for proper healing because it is a tendon to bone connection dealing with interlocking the fibers back into the bone. The Z-plasty weakens the structure of the tendon by cutting it in half which does not heal back to its original thickness.²⁴ The tenotomy has a higher probability of healing properly compared to the other two direct tendon repairs, but it does not guarantee that the tissue will reform in the orientation replicating the pre-operative mechanical strength and function.²⁴ The lesser tuberosity osteotomy also has problems in the healing process. Bone responds to mechanical loading to remodel and heal. These repairs must initially support the bone taken from the humerus, typically called a bone wafer or fragment, but must also transmit some mechanical loading which promotes remodeling and healing. Also if the bone does not heal, the repair will not revascularize, weakening the properties of the tendon. Moreover, the lesser tuberosity osteotomy technique is more suitable for younger patients with higher bone quality; with poor bone quality, the osteotomy could prove catastrophic due to lack of structural support.²⁴ Studies have been performed comparing the various techniques. *In vitro* mechanical testing, which will be

described in detail later in this manuscript, has compared the structural properties and clinical evaluations have examined surgical outcomes, because clinical success is the ultimate goal.

Clinical evaluations using ultrasound have shown that abnormal subscapular tendon-to-tendon healing correlated to a loss of isometric and isokinetic internal rotation strength, as well as to higher Disabilities of the Arm, Shoulder, and Hand (DASH), assessment scores.²² In an attempt to quantify the disability of upper extremity conditions, the DASH asks individuals about difficulties performing daily activities.¹⁹ Many reports show a significantly lower frequency of subscapular dysfunction with a lesser tuberosity osteotomy compared to a tenotomy.^{13, 23, 32, 34} All current osteotomy techniques rely on bone-to-bone, rather than tendon-to-tendon or tendon-to-bone healing. A recent retrospective study found that the incidence of complete subscapularis tears was 7 out of 15 in a tenotomy group while the incidence in an osteotomy group was 2 out of 24.³⁸ Furthermore, validated functional outcome scores were clinically and statistically better in the osteotomy repair groups.³⁸ The data suggested that the lesser tuberosity osteotomy technique more reliably produced suitable clinical outcomes and was thus the focus of the current study.

2.5.2 Lesser Tuberosity Osteotomy

Osteotomy repairs can be grouped into either tension-band or compression repairs.^{13, 32} In a tension-band repair, the suture grasps the tendon at the bone interface, travels over the lesser tuberosity, and attaches laterally to the bicipital groove through bone (Figure 2 A). As indicated in the figure, the technique generates a compressive force at the osteotomy site with a “hinge”-like effect located lateral to the osteotomy.^{13, 41} In contrast to the tension-band, the compression repair holds the osteotomy with circumferential sutures around both the implant and the lesser

tuberosity fragment (Figure 2 B). Unlike the tension-band repair, the compression repair “hinge” is located medially and the fragment could tilt in a manner detrimental to the repair. In a compression-suture repair, subscapularis muscle contraction could potentially open the repair site, whereas in a tension-band repair, relaxation of the subscapularis muscle could open the repair site.⁴¹

Another facet of the lesser tuberosity osteotomy repair is the size of wafer to remove from the humerus during the osteotomy. Gerber et al. reported that a lesser tuberosity osteotomy prevented, or limited, subscapular dysfunction and recommended an osteotomy (wafer) thickness of 5 to 10 mm.¹³ Concern has been expressed about repairs with osteotomy wafers that are either too thick or thin; Ponce et al. attributed clinical subscapularis repair failure to an undersized wafer.^{14, 32} Furthermore, suture tearing through the osteotomy fragment is a commonly observed *in vitro* failure mode.^{15, 23, 32, 41} No guidelines in the literature have been established regarding the ideal osteotomy thickness. Furthermore, the effect of fragment migration on the integrity of the osteotomy site is not known. One would assume that a smaller osteotomy would have a smaller margin for error and would become completely displaced before a larger osteotomy undergoing the same displacement. This data does not exist in the literature and is a critical factor in determining guidelines for ideal osteotomy thickness.

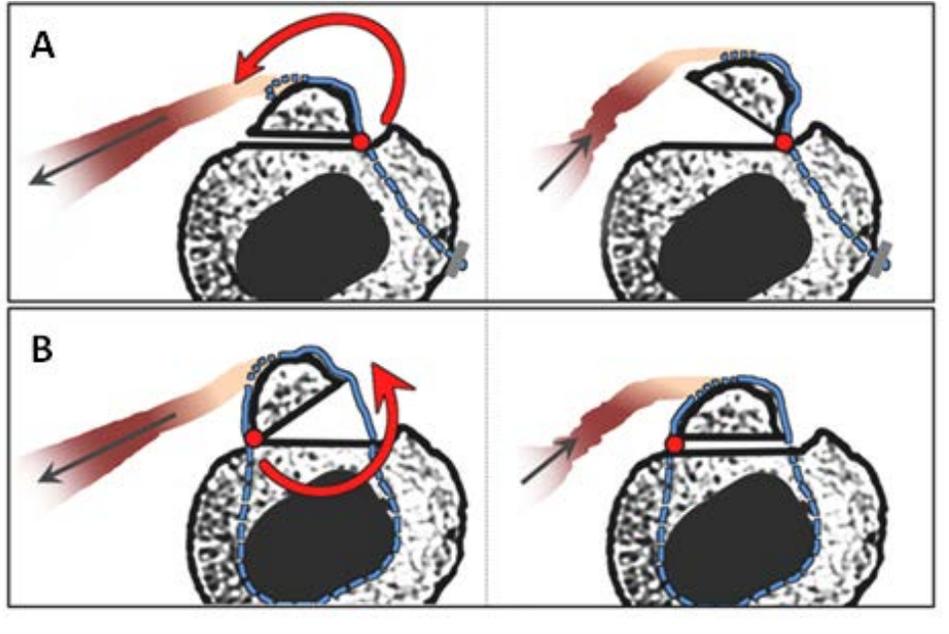


Figure 2: A schematic illustrating the two common repair techniques.

2.6 PREVIOUS WORK ON MECHANICAL TESTING OF LESSER TUBEROSITY OSTEOTOMIES

Mechanical studies have tested the different subscapularis repairs *in vitro* to quantify the structural properties of these repairs. Ultimately we would like to produce a construct that mimics the native subscapularis tendon. Ponce et al. in 2005 tested the osteotomy, tenotomy and subscapularis peel in cyclic loading and then loaded the repairs to failure while measuring movement at the repair site. To perform the experiment, a cadaveric humerus and attached subscapularis specimen was given one of the three subscapularis repairs. For the lesser tuberosity osteotomy, the humeral stem was cemented and given a compression repair with four suture

bands. Each humerus was mounted to a material testing system in a position that mimicked 45° of shoulder abduction and neutral (0°) rotation. The testing parameters for subscapularis repairs had not been defined in literature at the time and were thus derived from testing on the supraspinatus. Cyclic loading at 1 Hz for 3000 cycles was performed to 100 N, which was the estimated force to resist from expected passive internal rotation contraction force during the early postoperative period. The 3000 cycles was an estimate based on physical therapy protocols loading the shoulder for 70 repetitions per day for six weeks. Then load to failure was performed at 33 mm/s. The loading rate was derived from an estimate observed with daily activities. During the test, displacement was measured using a 9 mm differential variable reluctance transducer. Ultimately they found that the osteotomy allowed the least displacement (0.88 ± 0.54 mm) in cyclic loading and had by far the highest maximum load to failure (738 ± 261 N); however, all repairs had higher maximum loads than the 250 N estimate of maximum force production of the subscapularis.^{6, 31, 32} Concerns lay with the method of displacement measurement, which was not well described, with the age of the cadavers used, which was not reported, with validation of osteotomy size, which was not measured, and with the use of bone cement, which could artificially increase the load to failure values and which is used less frequently in TSA.

Van den Berghe et al. in 2008 analyzed osteotomy, tenotomy and subscapularis peel. The tension repair was used for the lesser tuberosity osteotomy and humeri were cemented in a custom test frame. The specimens (avg. age: 80 yrs.) were oriented to mimic neutral rotation with a linear force on the subscapularis tendon. The specimens were first preloaded to 10 N, then loaded to 150 N for 500 cycles at 1 Hz, and finally loaded to 300 N for 1,500 cycles or until failure; no load to failure was performed. After the cyclic loading, it was shown that the

tenotomy and osteotomy were far superior to the subscapularis peel technique and that osteotomy had higher cycles to failure than the tenotomy.⁴¹ The Van den Berghe study did not attempt to measure displacement and used a visual observation of gap formation to classify performance with three categories: pass, partial fail, or fail. Furthermore, the specimens used were not paired or matched and thus differences in bone and tendon quality could have biased the results. The authors made a comment on the size range for the lesser tuberosity osteotomies, but did not make an attempt to validate the osteotomy fragment sizes.

Van den Berghe's research spurred a study by Krishnan et al. in 2009 who tested two compression repairs and a tenotomy to determine if the addition of more sutures to compression repairs would improve the structural properties. This study involved no humeral implant; all drill holes were medial to the usual location of the implant. The specimens (avg. age: 53 yrs.) were repaired and mounted into an MTS to simulate 45° abduction and neutral rotation for cyclic loading. The test consisted of loading the repairs incrementally by 180 N every 400 cycles until failure was observed. Displacements were not measured: only gross movements were assessed visually. Mechanically, the osteotomies had the superior performance in cyclic testing and ultimate load to failure, however the osteotomy repair with two times as many sutures was not superior to the other osteotomy repair.²³ The subjective measurement of repair failure was a concern because the observation could be highly variable, and lack of a humeral implant was also a limitation. It is of interest that addition of compression sutures did not significantly increase the structural properties of the repair. The authors commented on the approximated range of osteotomy size, but did not actually measure the size.²³

Van Thiel et al. in 2010 compared the osteotomy, tenotomy and subscapularis peel techniques against each other in cyclic testing. The tension-band configuration of osteotomy

repair was used and a humeral implant was installed during preparation. This study quantified the bone mineral density of the specimens using DEXA scans. The specimens (Avg. Age: 57 yrs.) were loaded in neutral humeral rotation to 100N at 0.5 Hz for 150 cycles and then loaded to failure at 1 mm/s. Displacements were measured using an optical tracking system and failure modes were placed into three categories. The displacements (1.4 ± 0.4 mm) and maximum loads (543.3 ± 187.4 N) of the osteotomy were not different from the tenotomy or subscapularis peel. The osteotomy fragment sizes were not measured and the displacement calculations recorded the displacement from the peak of the first cycle of loading to the peak of the last cycle. This technique could potentially eliminate any displacement occurring in the initial cycle of loading. The cyclic test was also only 150 cycles, which is much less than the previous studies: fatigue testing usually consists of many more cycles.

One study, by Heckman et al., directly compared the two osteotomy techniques, tension and compression. These repairs had no humeral component and were mounted in an MTS to simulate neutral abduction and rotation. The dimensions of the lesser tuberosity osteotomies were quantified using digital calipers, which estimated the thickness to be 8.0 mm for both test groups. The specimens were preloaded to 10 N then cyclically loaded to 180 N for 500 cycles at 1 Hz; no load to failure was performed. Displacements were measured using a 9 mm DVRT attached to the bone fragment and the humerus. Analysis revealed that the compression repairs (4.6 mm & 632.3 N) were superior to the tension repairs (6.9 mm & 510.9 N) in that they displaced less under cyclic loading and produced higher load to failure.¹⁸ Both techniques had adequate ultimate load to failure, i.e., greater than the 250 N seen in the native subscapularis contraction, however the displacement values for each technique revealed more movement than desired. The displacement for the 500 cycle load test reached the 5 mm threshold deemed

detrimental by clinicians. Weaknesses of the study were that no implant was used to simulate a total shoulder replacement and that the cadavers used were younger (54 yrs.): age is factor because bone quality and structural properties deteriorate with age. Concerns existed with displacement measurements using DVRT's because the device must be aligned with the line of action if the recorded value is to match the actual value. Reduction of the wafer movement is one goal of active research in the lesser tuberosity osteotomy research.

The most recent study by Giuseffi et al. in 2012 found no differences between lesser tuberosity osteotomy and tenotomy.¹⁵ The specimens (No age data) were prepared with a compression osteotomy and loaded to 100 N for 3000 cycles at 1 Hz in neutral rotation and 45° of shoulder abduction. The repairs were then loaded to failure and displacements were measured throughout the testing using a DVRT. The displacement (1.8 ± 0.6 mm) and maximum load (447 ± 89 N) of the osteotomy was not higher than the tenotomy group, unlike previous reports.¹⁵ The osteotomy fragments were estimated to be 4-5 mm thick, but this was not validated. Concerns with this study involve the absence of reporting the age of the specimens and lack of osteotomy size validation. The literature overall supports the lesser tuberosity osteotomy technique as the superior method for subscapularis fixation, although similarities do exist with other techniques. Clinically the osteotomy technique seems to have a higher rate of success in comparison, however improvements on the structural properties of these repairs is warranted and is thus the goal of this study.

2.7 IMAGING

To quantify the osteotomy fragments created in this study the robust technique for imaging bone, computed tomography (CT), was utilized. Medical imaging uses different types of electromagnetic radiation to create contrast and image soft and hard tissues. X-rays provide contrast in an image as they are absorbed by tissues in the body and different tissues absorb the x-rays at different rates. Bone in particular absorbs much more than any other tissue in the body and thus x-ray is ideal for bone imaging. To further extend the power of the x-ray, CT is utilized to create a three dimensional scan of the tissue. CT works by taking hundreds of plane x-rays and organizing them in a manner that produces an image volume, a visual representation of the tissue using the absorptive properties of the x-rays. To create a CT volume one take a series of x-rays in the same plane to make a sinogram which is then analyzed with convolution backprojection to create one slice of the volume.³³ A series of slices of are compiled to create the CT scan and these are organized into Dicom images. Dicom is an image format that stores and organizes the information about the image scan so it can be viewed and utilized later. Information about the physical distance of the object being imaged, the imaging parameters, and thickness between image slices to name a few.

Once a Dicom CT image volume is created of the object there are several ways to analyze the information. One method is to use the information stored in the Dicom to create a solid computer model that is an accurate representation, within 0.2 mm, of the object that was imaged.^{9, 35} To do this the Dicom image volume is loaded into image segmentation software; for the purposes of this experiment, Mimics (Materialise Plymouth, MI) was utilized. Once imported the different structures in the image can be isolated by highlighting the pixels of interest. Isolating the desired structures in every slice of the volume will lead to segmenting that structure

out of the volume. Further processing can create a solid computer model from this segmentation where the software meshes the segmented object and creates a three dimensional surface. Using the information from the Dicom images this solid model can be stored and manipulated in computer programs and is an exact, properly scaled, replica of the imaged structure.¹⁷ The solid model created in this experiment to analyze osteotomy sizes was created by tessellating small polygons onto the surface of the segmented object. After creation of this model one can make modifications in other computer programs to evaluate the response of certain variables on the geometry of the imaged object to produce applicable data and further the understanding.

2.7.1 Bone Mineral Density Estimations

The lesser tuberosity osteotomy technique involves fixation of the tuberosity fragment to the humerus with suture. This fixation relies on the structural support of the bone and assumes the suture will not create stress concentrations and simply cut through. Bone quality can be an issue with cadaveric specimen and thus it is good practice to evaluate the bone quality to know if it could have a potential effect on the outcome. Only one of the studies involved with lesser tuberosity osteotomy quantified the bone quality¹², and this information could be a key factor in repair integrity. There are several ways of measuring bone quality with medical imaging: Dual-energy X-ray absorptiometry (DEXA), Quantitative Computed Tomography (QCT), micro Computed Tomography (μ CT) and high resolution magnetic resonance imaging (hrMR) to name the most common techniques.^{11, 33} The calculation typically made is an estimate for bone mineral density, the higher the bone mineral density the greater the structural and mechanical properties of the bone.²⁰ The DEXA technique is the most common as it is fast and uses lower doses of radiation.³³ DEXA is capable of accurately quantifying the bone mineral density, however, it

does not offer three dimensional or local analysis.¹¹ QCT, μ CT, and hrMR are great tools for assessing the quality of the bone, however these methods are time consuming and expensive. An alternative to these approaches is a calculation of the bone mineral density based on the thickness of the cortical bone. Tingart et al. established a significant correlation with the bone mineral density of specific regions, i.e. lesser tuberosity, on the humerus to the cortical thickness of the diaphysis of the humerus.³⁹ This study utilized this relationship as the only method available for bone quality quantification was standard computed tomography (CT) scans.

3.0 METHODS

3.1 PROJECT OVERVIEW

Twelve matched-pairs of fresh frozen cadaveric shoulders, average age of 75 with six males and six females, were CT imaged to determine the tuberosity height and to estimate bone mineral density (eBMD). In each pair, the sides were randomly assigned for either a thick or thin osteotomy and then rescanned to quantify wafer thickness. Each matched-pair underwent a TSA with the same osteotomy repair. Six pairs were repaired with 2 compression sutures (Compression) and the remaining six with 2 compression sutures and one tension band suture (Tension). The repaired humeri were mounted in a uniaxial test machine in order to load the repair anatomically. Each specimen was loaded once to 100 N while tracking displacement of the bone wafer using a video system. Cyclic loading was then performed from 25 N to 100 N at 1 Hz for 3000 cycles after which the specimen was loaded to failure. The 3000 cycle test simulated 6 weeks of post-operative rehabilitation. Displacements were computed as the difference between the markers on the osteotomy wafer and the humerus, in the direction of the applied force. Measurements included: initial displacement (cycle 1), cyclic displacement (cycles 2-3000), overall total displacement, and cyclic amplitude (average displacement per cycle). A partially nested two-way ANOVA tested for differences between groups; significance was set at $p=0.05$.

3.2 STUDY DESIGN

One side of twelve matched-pair cadaveric shoulders was randomly assigned for a thick osteotomy (100% of lesser tuberosity height) while the other side was assigned for a thin (50% height) osteotomy. Each matched-pair underwent TSA with the same osteotomy repair: both sides of the matched-pairs were randomly given the same repair, 1) two compression-sutures or 2) two compression-sutures plus one tension-suture. This procedure created four groups of six paired specimens (Figure 3). Six pairs were repaired with two compression-sutures (Compression) and the remaining six, with two compression-sutures and one tension-band suture (Tension). This resulted in four experimental groups with six specimens each: Group I–Thick/Compression, Group II–Thin/Compression, Group III–Thick/Tension, and Group IV–Thin/Tension (Figure 3). The average age of all of the matched-paired specimens was 75.2 (\pm 7.8) years ranging from 61 to 83. (Table 1 - Results Section). There were six male and six female specimens from which the pairs originated, each group had three males and three females (Table 1).

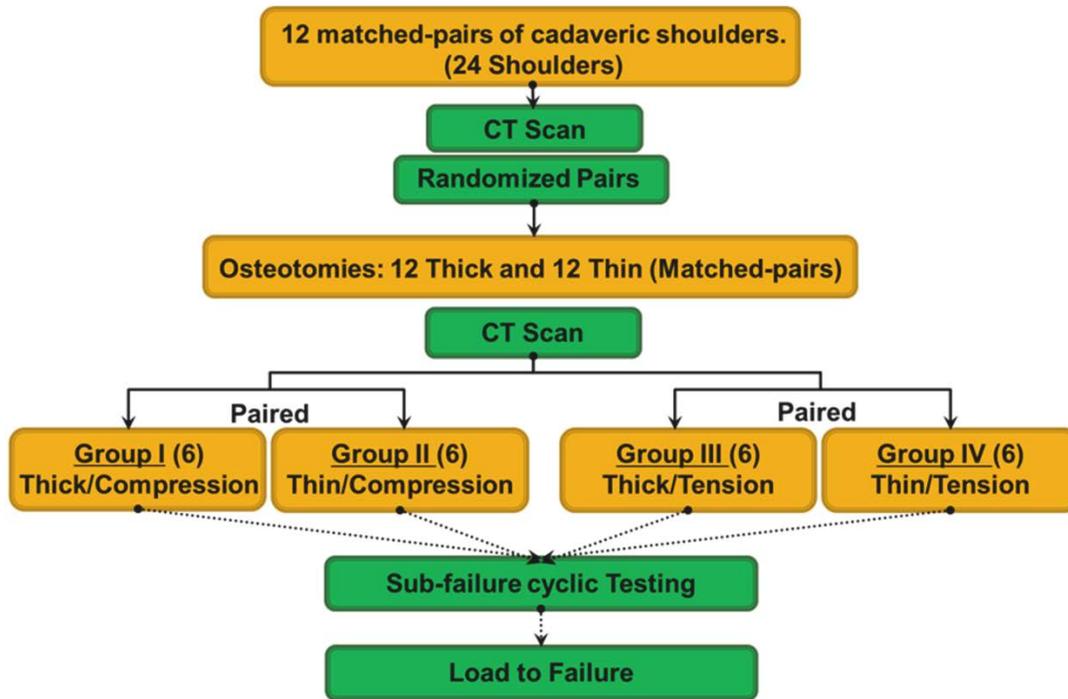


Figure 3: A schematic showing the partially nested experimental design.

3.3 CADAVERIC TISSUE

This study involved *in vitro* testing of human cadaveric tissue for quantification of lesser tuberosity osteotomy behavior. Cadaveric tissue has its limitations for the applications to the *in vivo* scenario as the tissue is no longer biologically active. The specimens used were fresh frozen as to mimic the *in vivo* tissue from as close a time point post mortem as possible. The test specimens would be kept frozen until the experiment could be conducted. Some of the potential issues with cadaveric tissue are the decrease in material properties of the bone, muscle, and tendons. Muscle and tendon can dry out and rapidly deteriorate in air thus keeping moist with saline solution while experimenting is essential. Bone material properties will not degrade as rapidly, however as most donors are older and the tissue is cadaveric the properties will be less

than live bone. As the lesser tuberosity osteotomy constructs rely on bone for fixation this is a limitation, however all variables being tested will be placed under the same limitations making comparisons possible.

3.4 OSTEOTOMY TECHNIQUE, BONE MINERAL DENSITY AND AREA

A main goal of the experiment was to create two distinct osteotomy groups within the matched-pairs; one composed of a thick and the other a thin osteotomy fragment (Figure 4). CT imaging was used to properly quantify the osteotomy dimensions of each specimen. The same scanner and scan parameters were used for the original scan as well as for a scan after the lesser tuberosity osteotomy. A Siemens dual source 64 slice scanner was used to create 1 mm thick axial slices reconstructed in the coronal and sagittal planes. Actuation was set at 120 Kvp while mA was set to 70 and modulated by CAREdose.

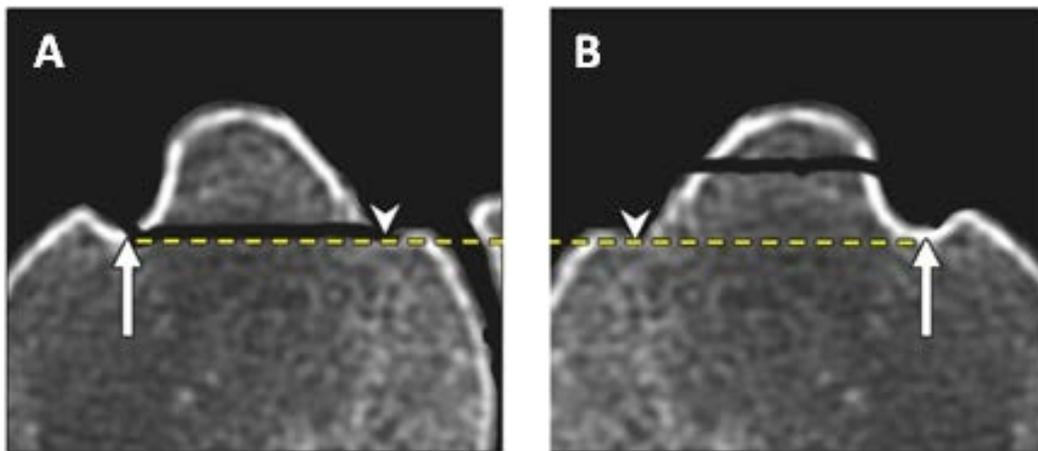


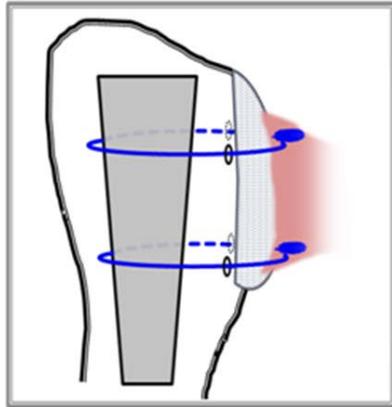
Figure 4: The figure shows the thick and thin osteotomies of specimen number 3025.

The original CT scan was used to quantify the height of the lesser tuberosity and these measurements were verified with caliper measurements taken from the specimen. The height was defined as the greatest perpendicular distance from the base line, where the base line connected the lowest point in the bicipital groove to the inflection point between the tuberosity and the humeral neck (Figure 4). The ideal thick osteotomy was 100% of the tuberosity height and the ideal thin osteotomy was 50% of the tuberosity height. The thick osteotomies removed the entire tuberosity using an oscillating bone saw by cutting along the base line (Figure 4A). The thin osteotomies were cut along a plane parallel to the base line by elevating the saw blade with a stack of thin metal plates to half the measured tuberosity height (Figure 4B). In the case that the thin osteotomy did not include the entirety of the tendon, the tendon below the osteotomy height was carefully elevated before sawing so that the entire tendon remained attached to the wafer. The original CT scans also allowed quantification of bone mineral density, as described by Tingart et al.³⁹ This process involved measuring the thickness of the cortical bone in the diaphysis of the humerus at four key points. The known relationship between the average cortical bone thickness of the humeral diaphysis and the lesser tuberosity bone density, $eBMD = 0.11*(Avg. Cortical Thickness)-0.05$, was used to estimate the bone mineral density of the specimens.³⁹ The specimens then underwent a second CT scan to measure osteotomy thickness and surface area of the cut radiographically. The surface area of the osteotomy was calculated from the CT image using Mimics software (Materialise, Belgium).

3.5 SURGICAL REPAIR TECHNIQUE

After humeral implantation (Figure 5), each matched pair was repaired with either two compression-sutures (Compression) or with two compression-sutures plus one tension-band (Tension). A press-fit hemiarthroplasty (Zimmer Anatomic Prosthesis, Warsaw, Indiana) was performed in standard fashion for each specimen. Prior to final seating of the humeral component, two parallel rows of 2 mm holes were drilled on each side of the osteotomy site: the lateral hole in the bicipital groove and medial hole between the osteotomy and neck cuts. Two strands of #2 FiberWire (Arthrex, Naples, Florida) were passed transosseously through the lateral holes, then through the respective prosthesis suture holes, and finally through the medial hole of drill-holes, thus placing the two sutures circumferentially around the implant. Slack in the sutures was removed while the prosthesis was pressed into the humeral canal. The lesser tuberosity, with the attached subscapularis tendon, was placed back onto the humerus in its anatomic position. All wafers were reduced in a similar fashion. After application of bone reduction clamps to anatomically reduce the wafer, the circumferential sutures were tied sequentially to maintain the reduction and compress the wafer (Figure 5 A). The Tension construct was created following the exact method described above, with the addition of a tension-band of #2 FiberWire. This tension-band suture grasped the tendon at the bone interface, passed over the lesser tuberosity and through a bone tunnel beginning at the lateral wall of the bicipital groove exiting on the lateral cortex; it was finally tied to an Arthrex Button (Arthrex, Naples, FL) (Figure 5 B).

5. A



5. B

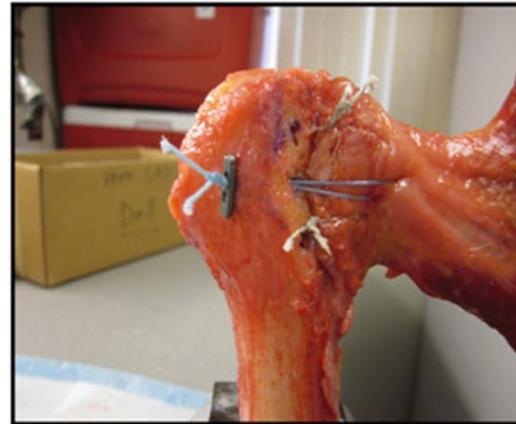
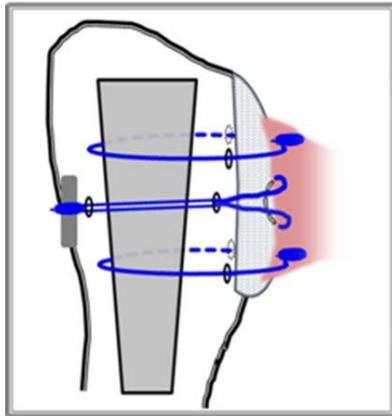


Figure 5: Diagram and photos illustrating the two repair types.

3.6 BIOMECHANICAL TESTING

Determination of what repair configuration for lesser tuberosity osteotomy is superior requires quantification of construct behavior. The aforementioned data from research involving the subscapularis muscle gives us criteria with which one can determine if a certain repair is adequate. The repair must be able to withstand the loads placed on it and it also must withstand those loads for a certain amount of time to allow for the tissue to heal. Thus the two variables we

would like to observe to compare repair configurations are the loads the repair can resist as well as how much the repair site moves under those loads. To measure these variables two systems are utilized; a material testing system and a video tracking system.

3.6.1 Material Testing System

A material testing system (MTS), as seen to the right in Figure 3, has the ability to apply known displacements and loads to materials while measuring either the load or displacement response. The system depicted is a servo hydraulic device that can apply loads or displacements in the axial, or vertical, direction as well as in torsion. The crosshead at the top calculates the movement of the actuators and the load cell at the bottom records the forces produced. The system is driven by a controller that supplies voltage to the motors, thus controlling the movement. The controller is equipped with a function generator so that one can move the middle actuator with numerous functions at a number of frequencies. The MTS can be controlled with either displacements or loads depending on the desired measurement. With the combinations of the appropriate fixation and this system, one can derive the properties of materials.

To adapt the relatively simple loading directions of this MTS to the highly complex geometry and potential positions of human anatomy one must be able to apply the loads to specimens in a meaningful manner. For example, if one wanted to examine the subscapularis muscle properties one would want to pull on the tendon in the same direction the muscle would pull on the tendon and in an anatomically correct shoulder position. To do this there are custom frames built that allow for this correct positioning as depicted in Figure 6, the frames are attached to the load cell and the actuator. The lower frame can translate in both directions in the horizontal plane as well as rotate about one of the axes as shown. This allows for all of the

degrees of freedom needed to load a subscapularis in numerous anatomically correct positions. Once in the correct position these frames must also be fixed rigidly so that once the test begins no movement can occur. The experiment requires all applied loads to be transferred directly to the specimen.



Figure 6: Image of the material testing system used for this experiment

3.6.2 Displacement Measurement

Displacements obtained from an MTS will suffice if the material being tested is sufficiently rigid. If this were true one could be confident the displacement recorded occurred only in that specimen at the region of interest; often in biological tissues this is not the case. Depending on the tissue being loaded the displacements can be quite variable and nonlinear. If one were to fix a bone into a clamp and pull on a muscle attached to that bone there would be numerous different displacements within each tissue that would sum up to the total displacement of the actuator. The bone might deflect a small amount under the loading, the tendon will stretch some amount, and the muscle will stretch a different amount. To accurately quantify the displacement of each there needs to be an additional measurement made so one can know the relative displacements of all the structures involved. The most common method to quantify these relative displacements utilizes optical displacement tracking systems.

Optical tracking systems utilize cameras that are related to the space around them by some sort of calibration method. This calibration could be as simple as a photograph with a scale and one can relate the pixels in the photograph to a distance to measure the displacements. More sophisticated tracking involves three dimensional space tracking of objects in any direction. In order to elevate the analysis to three dimensions a minimum of two cameras are needed, the cameras need to be synchronized and related to each other by a calibration. This calibration is more complex than simply placing a scale in view of the cameras in order to track points of interest. In order to register the cameras to each other a calibration frame is built that will dictate the distances calculated. Essentially one needs to know the same points and distances to those

points for each camera. The more points used for this calibration the higher the accuracy and decrease in the error. After a calibration, distance measurements can be made using the system. There is typically tracking accompanying software with the optical system that can analyze the video that is recorded of the experiment. This software utilizes contrast to aid in tracking movement in the created videos. When setting up an experiment from which displacement will be calculated it is important to place a contrasting marker on the desired area to be tracked. If done successfully one can automatically generate displacement quite quickly, however there are also manual tracking methods available where one can decipher displacements frame by frame. Depending on the desired scale of measurement the accuracy of the camera system can be a large factor and knowledge about the variables that affect accuracy is crucial in understanding the limitations of any particular tracking system.

The tracking system used in this project is from Spica Technologies (Spica Technologies Corporation Kihei, Maui, HI) and utilizes two cameras with DMAS6 motion analysis software (www.spicatek.com). One aspect of the tracking system that will affect the accuracy is the size of the calibration frame compared to the desired displacement measurements; they should be of similar scale. The associated calibration frame for this project is seen in Figure 7 and is 10 cm X 10 cm X 10 cm and contains 22 markers. The expected displacements for this project were within this range and were also not expected to be significantly small. Preliminary analysis of the accuracy of this specific system for the task of measuring osteotomy displacements observed in the literature to range from 0.8 mm to 6 mm was performed to ensure adequate accuracy. The first task was to create as accurate a calibration as possible which involved measuring the locations of each marker on the calibration frame using a CMM. This machine can accurately map, in three dimensions to an accuracy of 4 microns, the positions of each marker. After this

calibration file was create an analysis of camera position and accuracy was established by methodically changing the positions of the cameras with respect to one another and the calibration frame while tracking a marker undergoing a wide range of displacements. This marker was placed on a micrometer stage capable of accurate displacement in all three directions and moved 0.025, 0.25, 2.5, and 25.4 mm in each direction to determine the lowest accurate displacement measurement. The preliminary analysis demonstrated that the object to be tracked should be in within the volume of the calibration frame, cameras within 30 cm of the calibration frame, cameras at an angle between 30° - 90° , the perpendicular plane produced more reliable displacements than towards or away from the cameras, and the smallest accurate displacement was within 2% of 0.1 mm.

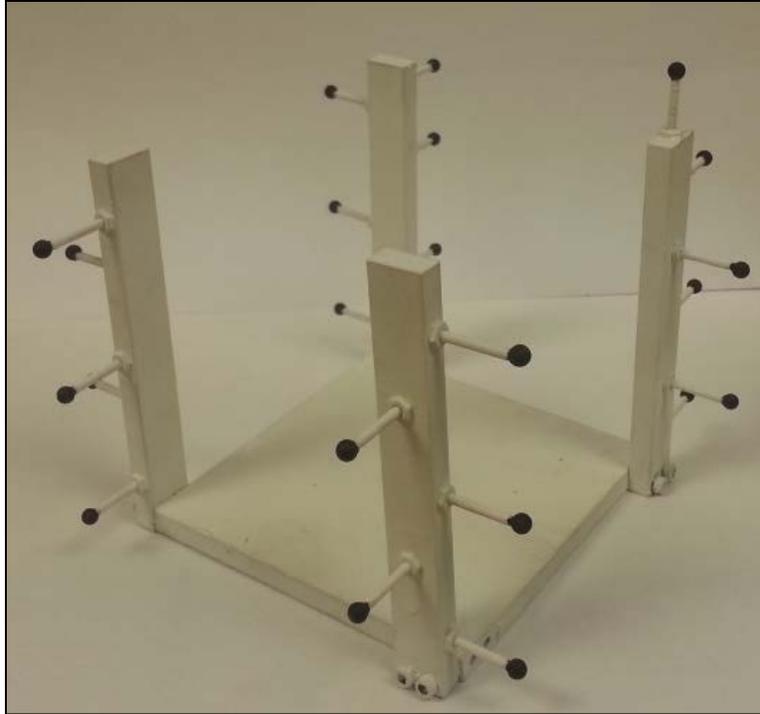


Figure 7: Image of the calibration frame used for this experiment

3.6.3 Testing

The humeri were potted in standard epoxy resin and markers were placed on the humerus and osteotomy bone wafer. They were then installed in a custom vise mounted to the base of a Material Testing System (MTS Systems, Eden Prairie, MN) (Figure 8). The position of the shoulder during testing simulated an anatomic position of 0° of abduction with neutral rotation, with the muscle's line of action oriented at 90° to the axis of the humerus. This allowed the subscapularis repair to be stressed in line with its muscle-tendon axis, similar to other subscapularis testing protocols as outlined previously.^{2, 18, 41, 42} A 1.5 kN transducer was used to quantify the load and a custom designed script in Matlab recorded and stored all biomechanical information.

The video motion analysis system recorded osteotomy displacement during initial and cyclic loading. Displacement was computed as the difference in movement between the markers on the humerus and the markers on the osteotomy fragment in the direction of the actuator loading the specimen, as seen in Figure 8. A custom script in Matlab, appendix B was written that computed the displacements from the CSV file output by the tracking system. The movement was quantified as initial, cyclic, or total displacement. Initial displacement was the amount of osteotomy fragment movement during the first cycle, while cyclic displacement measured the amount of movement from the second to the 3000th cycle. Total displacement was the sum of initial and cyclic displacements. The specimens were loaded with a 5N preload, and then cyclically loaded to 100 N at a rate of 1 Hz for all 3000 cycles, as previously described (Figure 9).³² The 100N load was deemed reasonable because the subscapularis muscle *in vivo* can generate 135 N during resistance to a 30N external rotation load.⁶ The number of cycles was based on an estimated six weeks in a physical therapy program.³² Movement of the osteotomy was tracked by comparing stationary humeral markers to the osteotomy edge or markers. Due to the small size of some thin osteotomies, the markers themselves were not useable for displacement calculations because no surface adequately represented movement of the bone fragment. For these specimens, the edge of the osteotomy was used to measure displacements. A pilot study was performed to create test measurements that reliably and accurately tracked the edge of the osteotomy and was validated.

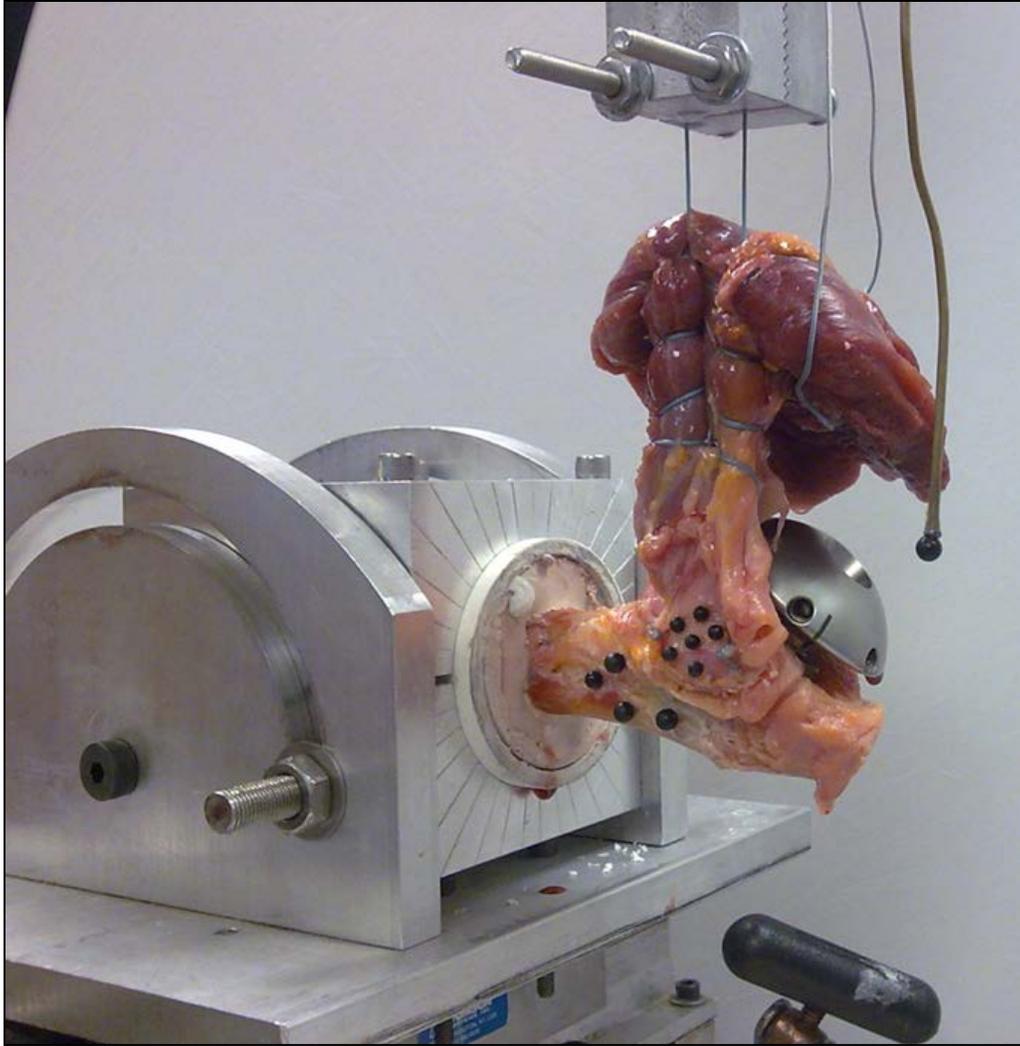


Figure 8: Photograph of the mechanical testing setup

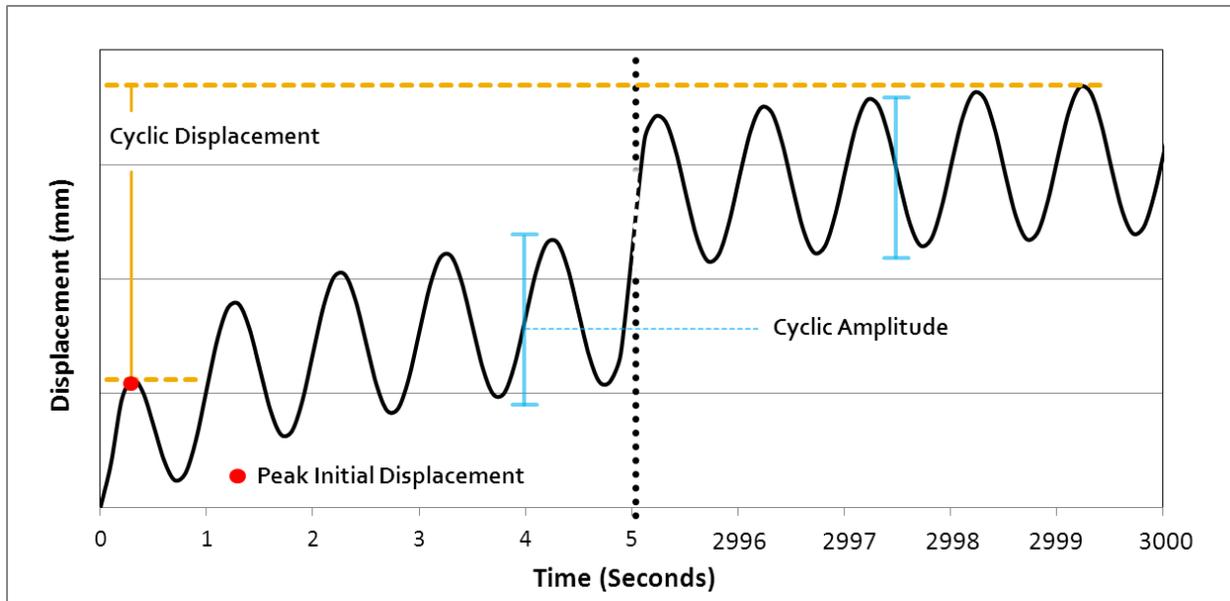


Figure 9: Schematic of cyclic testing protocol and subsequent calculations.

This pilot study involved manual tracking of the osteotomy edge during the mechanical testing. The first step in validation was to determine if the osteotomy cut site could be seen in all testing videos for all specimens. The next step was to determine if the locations chosen produced a point that was in fact on the osteotomy site; if the two points chosen for the same time point were off between the two cameras the point would not be on the osteotomy site, but some distance towards or away rendering the point chosen useless. The ultimate factor for validation was how the new osteotomy edge points displacements compared to actual marker displacements in the same area. After comparing these three steps and producing comparable displacements, the osteotomy edge tracking technique was used for small osteotomy fragments where markers placed on the bone-tendon interface were not an adequate representation of osteotomy displacement. The validation and procedure are outlined in Appendix D.

The specimens that remained intact after cyclic loading were tested for maximum load to failure. This test displaced the crosshead of the MTS at 33 mm/sec until the repair could no longer withstand significant load (Figure 10). Maximum load was the peak load value and the stiffness of each repair was calculated as the slope of the linear portion of the load-displacement curve. The mode of failure was recorded and categorized for each specimen.

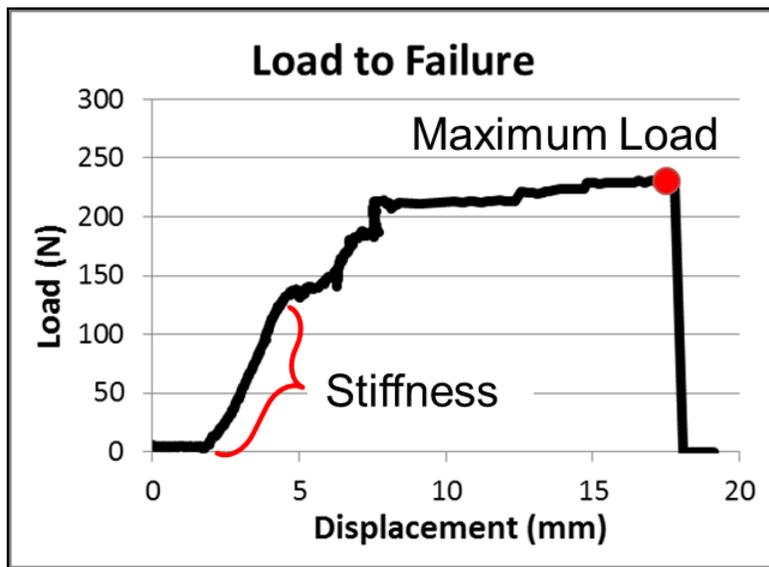


Figure 10: Load to failure output of a typical specimen with subsequent calculations.

After the cyclic loading, the contact area between the fragment and cut site was calculated in Matlab software (MathWorks, Natick, MA), Appendix C, by importing the osteotomy surface area, total displacement after testing, and tendon direction vector. To compute

those various parameters the CT scans were imported into Mimics software (Materialise, Plymouth, MI) where the osteotomy fragment and cut site were segmented out from the Dicom images. In a similar fashion the direction of subscapularis pull was determined by creating a line of direction off of the osteotomy fragment towards the scapula for all slices that included a piece of the osteotomy. This information was then imported into Matlab where the contact area could be measured by applying a translation to the osteotomy fragment along the cut plane in the direction of the subscapularis tendon; the overlapping area of the cut site is depicted in Figure 11. The osteotomy percent contact with the humerus was expressed as the ratio between initial cut area and the area of overlap after cyclic loading.

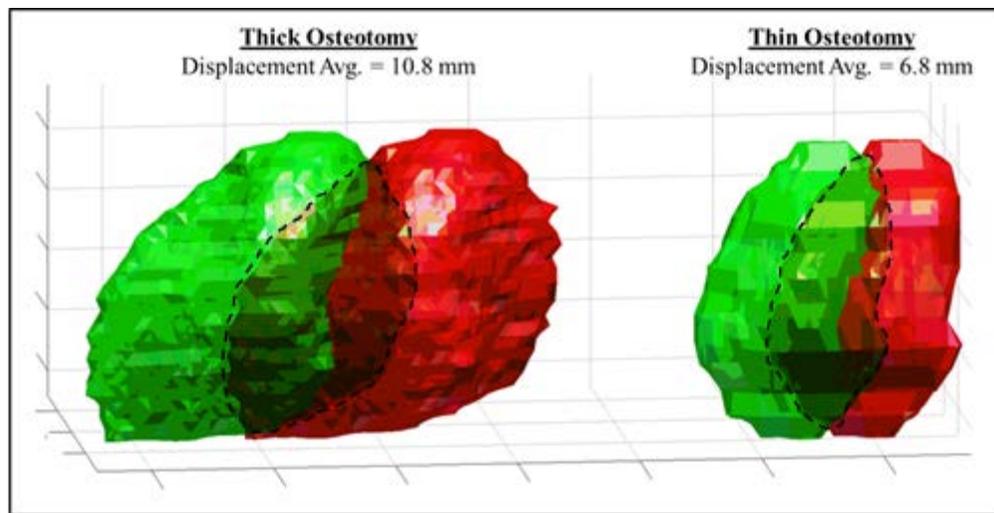


Figure 11: Diagram depicting the calculation for osteotomy contact area after cyclic testing.

3.7 STATISTICS

Statistical tests were performed using Minitab software (Minitab Inc. State College, PA). An analysis of statistical power was used to determine the minimum number of specimens needed. Previously published effect sizes for lesser tuberosity osteotomy repairs were used as a basis to determine that a sample size of 4.6 would provide adequate power ($\alpha = 0.05$ and $\beta = 0.2$) to detect differences in osteotomy displacement.^{18, 32, 42} The number of specimens per group used in this experiment was set at six to allow for experimental error and increase the probability of detecting differences.

The experiment, illustrated in Figure 3, was a partially nested design. The test was therefore a two-factor, partially nested in one factor, analysis of variance (ANOVA).²⁹ The ANOVA could examine osteotomy thickness and repair style and could find interaction between two independent variables. Tukey's post-hoc test was used to determine where significant differences occurred between the four groups if a factor proved significant. To analyze failure modes, a contingency table was created and analyzed using a Fisher's exact test, with SPSS software (SPSS, IBM Corp. Armonk, NY). Significance was set at $p = 0.05$ for all tests.

4.0 RESULTS

4.1 SPECIMENS

The average estimated bone mineral density calculated from the CT scans was 0.56 g/cm^2 . There was no significant difference in bone density between the between the thick or thin osteotomy groups ($p=0.71$) as seen in Table 1. The tension group was 8.4 years older than the compression group ($p=0.006$). Further, the compression group had a statistically higher eBMD than the tension group ($p=0.003$), which matched the age difference.

4.2 OSTEOTOMIES

The average lesser tuberosity height for all specimens was 10.9 mm (Table 1). The tuberosity heights were similar in all of the test groups with no detected differences ($p > 0.16$). However, the tuberosity height between specimens was significantly different ($p < 0.001$), so the osteotomy thickness was standardized by dividing it by the tuberosity height, described as the tuberosity percent. The average osteotomy thickness and tuberosity percent between thick and thin was significantly different, $p < 0.001$. The average tuberosity percent for the thick osteotomy groups was 82% (Range: 54-109%) whereas for the thin osteotomy groups were 37% (Range: 24-48%) of the tuberosity height. Osteotomy area between the thick and thin osteotomy groups differed

significantly ($p=0.008$), as thick osteotomies had a much larger cut area. No osteotomy differences between tension and compression repairs were detected ($p> 0.65$).

Table 1: Data from the experiment.

Table I: Experimental Data						
	Group I	Group II	Group III	Group IV	Osteotomy	Repair
Osteotomy	Thick	Thick	Thin	Thin	Differences	Differences
Repair	Compression	Tension	Compression	Tension	p-value	p-value
Demographics						
Age	70.6 ± 8.8	79.0 ± 4.3	70.6 ± 8.8	79.0 ± 4.3	0.999	0.006
eBMD (g/cm ²)	0.62 ± 0.09	0.49 ± 0.09	0.63 ± 0.08	0.52 ± 0.09	0.708	0.003
Sex	3 - M 3 - F	3 - M 3 - F	3 - M 3 - F	3 - M 3 - F	0.999	0.999
Osteotomy Data						
Tuberosity Height (mm)	10.76 ± 2.75	10.75 ± 1.26	10.88 ± 2.60	11.25 ± 1.67	0.164	0.889
Osteotomy Thickness (mm)	8.96 ± 3.10	8.49 ± 1.61	4.34 ± 1.39	3.87 ± 0.94	< 0.001	0.656
Tuberosity Percent	83.5% ± 20.9%	80.7% ± 22.0%	39.8% ± 8.0%	34.7% ± 7.9%	< 0.001	0.653
Thick vs Thin Percent	82.1% ± 21.5% (8.75/10.76)		37.3% ± 8.0% (4.11/11.07)		< 0.001	N/A
Osteotomy Area (mm ²)	424.4 ± 258.2	485.7 ± 270.5	187.9 ± 96.7	154.4 ± 93.1	0.008	0.872
Displacement Data						
Initial Displacement (mm)	9.88 ± 4.94	3.58 ± 0.75	5.11 ± 2.71	3.50 ± 0.75	0.011	0.024
Cyclic Displacement (mm)	2.39 ± 1.12	3.38 ± 2.73	4.22 ± 2.33	3.15 ± 2.17	0.914	0.666
Total Displacement (mm)	12.27 ± 3.03	6.96 ± 1.74	9.32 ± 2.52	6.65 ± 1.46	0.808	0.034
Percent Osteotomy Contact	22.9% ± 35.7%	46.7% ± 31.7%	22.9% ± 24.9%	36.6% ± 20.7%	0.431	0.251
Structural Properties						
Maximum Load (N)	249.0 ± 150.1	301.3 ± 134.5	234.7 ± 97.0	281.8 ± 45.8	0.670	0.401
Stiffness (N/mm ²)	45.00 ± 6.44	67.27 ± 15.92	46.39 ± 7.95	75.19 ± 16.52	0.102	0.032

4.3 DISPLACEMENT DATA

In all four groups, more than 50% of the total displacement occurred during the first cycle (Table 1 and Figure 12). Two thick/compression repairs failed during the first cycle, one at 67 N and the other at 100 N. All other specimens remained intact. This initial displacement varied between all four groups; there was a significant difference in displacement between the osteotomy thickness

groups ($p=0.011$), where the thin groups (avg. 4.3 mm) displaced less than the thick (avg. 6.7 mm). Displacements were similar in the tension repair groups, whereas the compression groups varied by a large amount. Statistical analysis determined that repair style caused a significant difference in initial displacement ($p=0.024$); the tension repairs (Avg. 3.5 mm) displaced less than compression repairs (Avg. 7.5 mm). The statistical test also determined that the interaction of osteotomy thickness and repair style was significant ($p=0.013$), meaning that the two variables affected one another. Further analysis revealed the thick osteotomy group with a compression repair displaced significantly more than the other three groups ($p<0.001$) during the initial displacement (Table 1). It should be noted that the specimen pairs did not have significantly different displacements ($p=0.65$), meaning the left and right side of each individual did not displace differently.

The cyclic displacements displayed little variability between groups (Figure 12). One thick/tension specimen failed at the 400th cycle while all other specimens completed all 3000 cycles. There were no differences due to osteotomy thickness or repair style and there was no interaction between thickness and repair style. The total displacement showed differences between groups. The thick osteotomy group had greater total displacement (9.6 mm) than the thin osteotomy group (8.0 mm), but this result was not significant ($p=0.808$). However, when comparing total displacement of the repair styles, the tension style repair (6.8 mm) displaced less than the compression style repair (10.8 mm) and this difference was significant ($p=0.034$). There was no interaction between the osteotomy thickness and repair style groups for the total displacement ($p=0.70$). The percent osteotomy area of contact (Figure 6) revealed no differences between osteotomy thickness or repair groups ($p>0.251$).

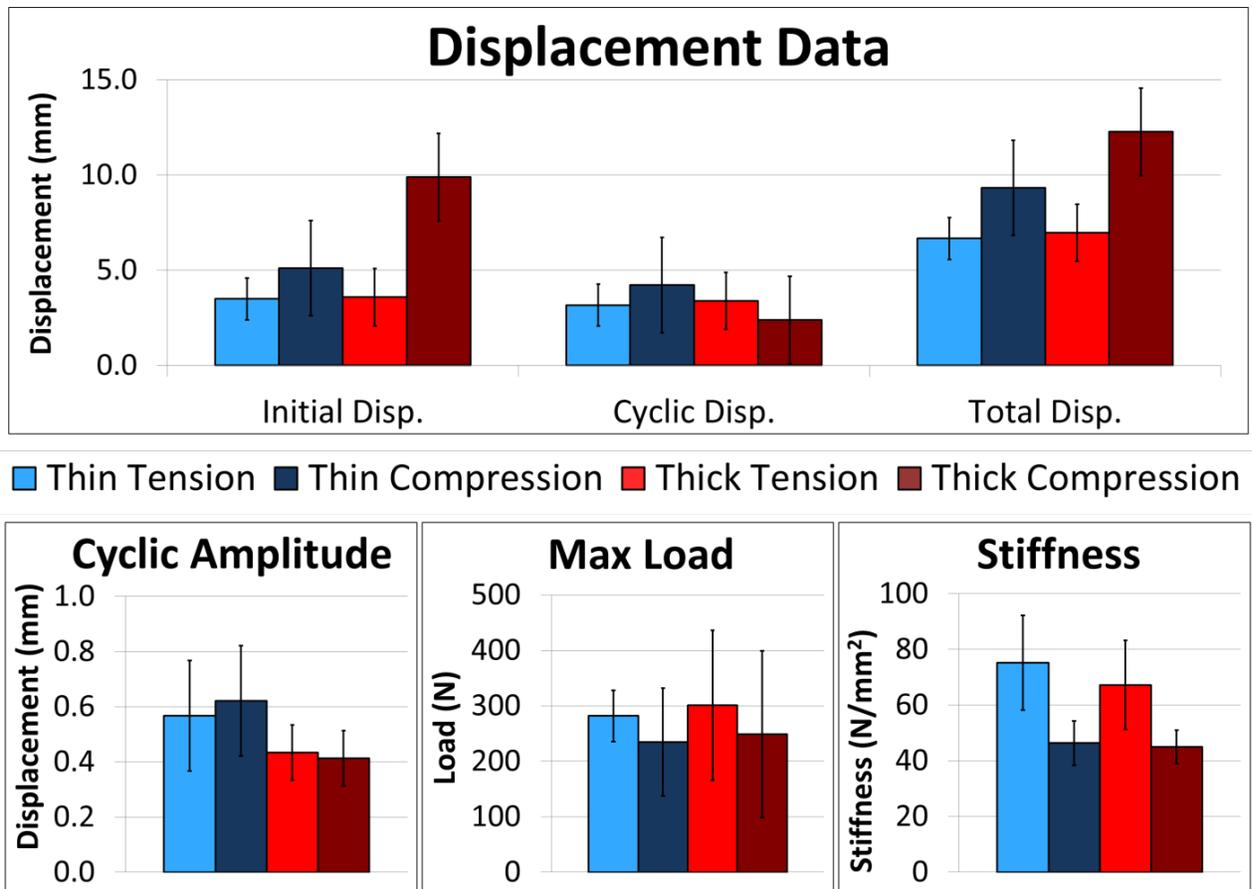


Figure 12: Results of the displacement and mechanical data for all tests groups.

4.4 STRUCTURAL PROPERTIES

All repair types produced similar average maximum loads (Table 1 and Figure 12). There were no differences detected between osteotomy thickness groups or repair groups. Stiffness calculation revealed no difference between thick (56.1 N/mm²) and thin (60.8 N/mm²) osteotomy groups; however, the tension repairs (71.0 N/mm²) were significantly stiffer (p=0.032) than the compression repairs (45.7 N/mm²).

4.5 FAILURE MODES

Four failure modes were observed during the experiment: failure by suture, osteotomy fragment, humeral neck fracture, and suture cutting through the humerus (Figure 13). Failure by suture involved direct failure of the suture material which included failure of the knots; osteotomy failure was defined as compromise of the osteotomy fragment in any manner. Humeral neck fracture involved failure of the bone in the humeral neck which was either fracture of the humerus or extracting of the lateral button through the bone. Finally, suture cutting involved slicing through the bone by sutures. The differences observed in failure modes were found to be significant ($p=0.001$), meaning osteotomy thickness and repair type related to the mode of failure. The most common failure mode for the thick osteotomies was suture cutting through the proximal humerus, 8/12 (66.7%). This failure mode only occurred twice in the thin group, 2/12 (16.7%). The most common mode of failure for the thin osteotomies was humeral neck fracture, 5/12 (41.7%), and this failure mode was not seen in the thick osteotomy groups. Failure through the osteotomy fragment also occurred only in the thin osteotomy groups, 3/12 (25%). Humeral neck fracture and suture cutting through bone were equal with 5/12 (41.7%), as the most common tension repair failure mode. The most common failure mode in the compression repair group was also equal in two categories: suture cutting through bone and suture failure, with 5/15 (41.7%) for each.

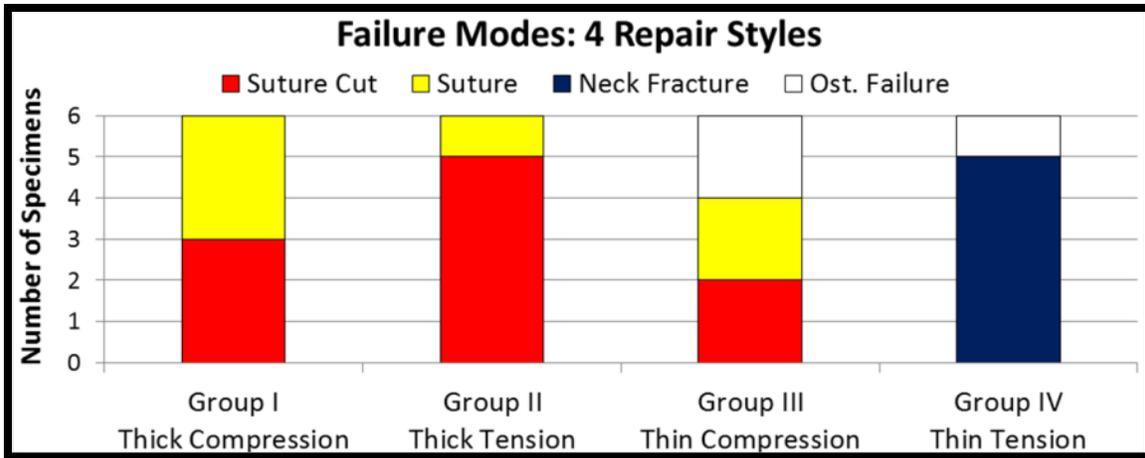


Figure 13: Frequency diagram for the failure modes observed during the load to failure test.

5.0 DISCUSSION

The demographic of the specimens used was highly representative of the population that will receive this type of procedure; the average age of the specimens was 75 years old and there were both males and females. The eBMD was similar to that of an age-matched population⁹. The experiment performed had a small sample size (N=24), that was further decreased by the fact that the specimens were paired. This pairing was strategically placed to eliminate variability between the testing variables. With a small sample size it is important to organize the testing variables appropriately as well as eliminate as much variability as possible between those testing variables. The partially nested experimental design organized the testing variables, thickness and repair style, in a manner that could examine the effect of those variables in the most efficient manner given the small sample size. The variability between testing groups was minimized, but was not ideal. This is to be expected when selecting from a random population. The ages, tuberosity thicknesses, and bone mineral density between the four test groups were not different, which is an ideal setup. However, upon further analysis there were differences found in bone mineral density between osteotomy thickness and repair style test variables. This occurrence is attributed to random chance and is taken into account when interpreting the results of those two variables. Significant variability was also found between each specimen when comparing the original tuberosity heights. This effect is attributed to natural differences between sizes of human beings and was accounted for by normalizing the osteotomy thicknesses. This normalization involved

categorizing the osteotomies differently; thick osteotomies would be 100% of the tuberosity thickness and thin osteotomies would be 50% of the tuberosity thickness. This created two groups, from paired specimens, that would be comparable as thin and thick bone fragments; which takes into account the overall size differences. The specimens created across the four testing groups were deemed comparable.

The first challenge of the experiment was to create consistent osteotomies. The use of the CT scans allowed for an easy method of analysis to gain knowledge about the tuberosity before the specimens even needed thawing. The thick osteotomies were easier to create than the thin osteotomies; however there was more variability in the thick osteotomy group. This could be due to the difficulty of sawing through a larger portion of bone and staying on the same cutting plane. The thin osteotomies often dealt with shaving off a small piece of bone. The thick and thin osteotomy groups were both lower in thickness than anticipated. This can be attributed to the difficulty in creating exactly sized, down to the millimeter level, osteotomies with a hand held bone saw. The difference in size between the thin and thick osteotomy groups, however, was quite pronounced and quite significantly different. This difference was planned and the thickness variable was created appropriately. The repair styles had very little variability as the same construct was used for either the tension or compression style repairs.

The displacement data is the most important piece of information in this study as it shows how these repairs hold together under anatomical loading. The 100 N cyclic loading mimicked sub-maximal contraction of the subscapularis, which would be imparted on the repair if a person was not limited after surgery. The initial displacement in this study contained a significant amount of displacement as observed in other studies. The findings here show that repair style and thickness are significant and they significantly affect one another. The reason for this can be seen

in that the thick compression repair performed significantly worse than the other three groups, and the thin compression also had higher displacement than either tension repair group. This means that the tension repair displaced less than the compression repairs and the thin osteotomies less than the thick osteotomies for the initial displacement. We were surprised by the high initial displacement of 9.88 mm in the thick/compression group compared to the other groups. The groups were similar in age, sex, and eBMD, so this difference was solely attributed to osteotomy height (Table 1). Further, two of the six thick/compression specimens demonstrated catastrophic failure in the first cycle. Catastrophic failure did not occur in any of the thick/tension, thin/compression, or thin/tension specimens. For this reason, a thick osteotomy stabilized with two compression sutures after implanting a press-fit humeral stem is clearly an insufficient technique.

The cyclic displacement was not different between the groups suggesting that all repairs displaced a similar amount from cycles 2-3000, no one combination displaced less. The total displacement tells the complete story of how well the repairs held together and this analysis revealed that only the repair variable was significantly different. The effect of the repair style combined with osteotomy thickness degenerates with time isolating the two repair styles. The final aspect of displacement data is the cyclic amplitude displacements where the thin osteotomies displaced more for each cycle than the thick osteotomies. This suggests the thick osteotomies are more stable, however when compared to the overall displacement that occurs with the thick osteotomies the effect of the difference detected in amplitude are minimal. This data suggests that the tension style repair is superior to the compression style repair when searching for minimal medial displacement. Thin osteotomies are initially different than thick osteotomies, but over time the behavior of the two thicknesses converge and do not differ.

This study found a significant amount of total displacement in all four groups. However, the lesser tuberosity fragment and the proximal humerus maintained 23% to 47% of the original contact area (Figure 11) during the simulated six weeks of rehabilitation with no support from other structures or healing. The study showed that 50-80% of the total displacement occurred in the first cycle for all groups indicating a large amount of inherent slack in the system that one would assume to be detrimental. After this slack was removed the repairs displaced less, the remaining displacement only accounted for 20-50% of the total displacement. A recent tension-band cadaveric study also reported large initial displacements of 4.6 mm and cyclic of 2.3 mm from cycles 2-500, attributed to slack in the repair.¹⁸ It is almost certain that early motion at the osteotomy occurs *in vivo*, and should have deleterious effect on healing, yet a lesser tuberosity nonunion is uncommon.^{13, 22, 32, 34, 38} Figure 11 shows that bone-to-bone apposition still occurred despite osteotomy site motion; this contact seems to be enough to stimulate tuberosity healing *in vivo*.

The final pieces to analyze are whether or not the structural properties measured are different. The repair configuration with superior structural properties would be of high importance in selecting the superior repair. All repair constructs produced adequate maximum loads when compared to the estimated maximum contraction load of the subscapularis, 250 N. The statistical analysis showed no difference in maximum load. An *in vivo* study estimated that the subscapularis muscle generates 135 N while resisting a 30 N external rotation force.⁶ All repairs paper should be able to withstand these *in vivo* loads and not completely fail, however it is key to pair the load data with the displacements. Overall the displacements were higher than desired, however the tension groups displaced less while undergoing the same loading. This is

evident in the displacements being lower and the stiffness being higher in the tension groups. The ultimate factor for success is the displacement, thus improvement in all repairs is needed, however when comparing these four groups it can be said the tension groups with either thickness are the superior repairs.

The literature reports *in vitro* load to failure ranging from 279N to 738N (Table 2).^{2, 15, 18, 23, 32, 42} Comparison between the studies should be made with caution because there are significant differences in cementing, canal broaching, and repair technique (Table 2). Cementing, increasing the number of repair sutures, and increasing suture size will increase the repair stability, while canal broaching has the opposite effect. The present study tried to replicate the most common clinical scenario: a seventy-year-old patient treated with a press-fit humeral component. The older demographic, lower number of sutures, smaller sutures, and lack of cementing can account for the lower load to failure numbers in our study when compared to the literature. One notable concern is present in the mode of failure data with a large number of failures occurring due to suture pulling through the humerus. If the sutures sawed through the bone and were still looped around the implant, then a high load could be seen as it is not clear when this sawing first occurred and at what load. The mode of failure data in the literature does not attempt to classify the failure at this level of detail, it is simply listed as bone failure and it is a common occurrence. The loads reported could be artificially high as most studies used larger sutures and a larger number, thus increasing the ultimate loads while the repair could have failed long before the reported maximum.

Table 2: Comparisons from other publications.

Article	Average Age (Yrs.)	Cement Used	Canal Broaching	Repair Technique (No. Sutures, Type)	Load to Failure (N)
Ponce et al. ³¹	N/A	Yes	Yes	Compression (4, #5)	738 ± 261
Van den Berghe et al. ⁴¹	80 ± 4.5	No	No	Tension (2, #2)	300*
Krishnan et al. ¹¹	53 ± 9	No	No	Compression (4, #5) Compression (8, #5)	448 ± 125
Van Thiel et al. ⁴²	57 ± 8	No	Yes	Tension (2, #5)	543 ± 187
Heckman et al. ¹⁷	54 ± 7	No	No	Tension (2, #2) Compression (4, #2)	571 ± 180
Giuseffi et al. ¹⁴	N/A	No	Yes	Compression (4, #5)	447 ± 89
Current Study	75 ± 8	No	Yes	Compression (2, #2) Tens. & Comp. (3, #2)	265 ± 106

The mode of failure data showed that 8 out of 12 thick specimens failed by suture pulling through the humerus, this mode of failure only occurred in 2 out of 12 thin specimens. Furthermore, 5 out of 12 thin compared to 0 out of 12 thick osteotomy specimens failed by fracture at the humeral neck. This type of failure compromised the humerus before the repair site fully displaced. This mode of failure has not been reported in the clinical setting. The average maximal load to failure of the 5 fracture specimens was 293.7 N and the maximum *in vivo* subscapular contraction has been estimated to be as high as 250 N so the native subscapularis may not be able to produce a proximal humeral fracture.⁶ It also may be that an *in vivo* fracture does not occur because of proximal humeral hypertrophy in which the present *in vitro* study cannot model. It should also be noted that within the humeral fracture failure group there were two distinct ways of compromising the humerus; fracture of the neck itself and the lateral buttress plate of the tension band pulling through the humerus. These both occurred at the

aforementioned high loads and were deemed similar enough in comparison to the other failure modes. More notably the thick osteotomies had a higher amount of repair suture pulling through the humerus at the osteotomy cut site. Thick osteotomy fragments removed more cortical and cancellous bone from the native humerus thereby weakening the repair, risking early suture pull out. Other authors have reported that the presence of cortical bone between the head and neck cuts improved repair strength.²³ One finding of great importance is that the thick osteotomies did not produce different structural properties compared to thin osteotomies. One concern previous to this experiment was the integrity of the thin osteotomy. The data suggests that a thin osteotomy is nearly equivalent to a thick osteotomy and failed osteotomy fragments might not be as large of a concern as previously thought.

Ponce et al. used thin (4-5 mm) osteotomy fragments and showed lower displacement values (0.88±0.54 mm) than the present study.³² However, a direct comparison to the present work must consider that Ponce did not validate the osteotomy size, that the fragment was stabilized with four #5 FiberWire sutures instead of two or three #2 FiberWire sutures, and that the humeral stem was cemented (Table 2).³² The current work agrees with Ponce et al. in the use of more sutures as a means to improve fixation. Any use of bone cement would stabilize the compression sutures and prevent early suture cutout in the proximal humerus. In the preliminary work, using cementless humeral stems, suture cut out through the proximal humerus when tying down the compression sutures was observed if the sutures did not pass through the manufactured implant holes. The supplied implants only contained two machined holes through the implant for suture. Thus, for a cementless implant, the addition of a tension suture instead of a further compression sutures tended to stabilize the repair without damage to the proximal humerus.

In a clinical paper, Gerber, et al, recommended an osteotomy thickness of 5-10 mm.^{13, 14} They surmised that a larger osteotomy would place the repaired tuberosity directly onto the metal implant instead of the proximal humerus and that a smaller fragment would risk failure by suture pulling through the osteotomy wafer.^{13, 14} This study agrees that a large osteotomy fragment can lead to an exposed humeral stem, but more importantly, that a larger cut weakens the bone. Additionally, suture pulling through the thin osteotomy was an uncommon mode of failure in our tests. Based on the findings and the relevant literature, the ideal subscapularis osteotomy size should be 40-50% of the tuberosity height measured from the base of the bicipital groove, or 4-5 mm starting at top of the tuberosity in an average sized patient.

Adding a tension-band suture to two compression sutures resulted in less initial displacement, smaller total displacement, and a stiffer construct (Table 1). The tension groups performed better than the compression groups despite having significantly higher age and corresponding lower eBMD. The superior performance of tension repair groups is not a surprising finding, given that this construct combines two different biomechanical repair techniques, illustrated in Figure 2. In theory, the tension-band compresses the osteotomy during subscapularis contraction, while the two compression sutures hold the osteotomy together during muscle relaxation. However, the superior biomechanical properties with the tension band could conceivably be attributed to the additional third suture, and not to the tension-band effect. A third group, which was not possible with the paired specimens, would have been required to test this difference. Further, as described, the addition of a third suture to these constructs with the given implants was deemed detrimental as there was no third hole through which to pass the third suture. The addition of this third suture only seemed to compromise the repairs as it would slice through the humeral bone when simply tying the knots. Future work is needed to truly

evaluate whether this limitation affected the outcome; however, previous studies have highlighted that more compression sutures do not increase repair stability.^{23, 41} Not controlling for this variable certainly detracts from the findings; however it was deemed a necessary weakness of the study.

The overall ideal repair was a lesser tuberosity fragment measuring 40-50% of the tuberosity height or a 4-5 mm osteotomy in an average patient, with a combination of compression and tension sutures. A 40-50% wafer preserves proximal humeral bone stock leading to less suture pull out. Adding a tension-band to the repair further increases fragment stability. The most common mode of failure in the thin/tension group was a proximal humerus fracture at high load, leaving the subscapularis repair site intact. The thin/tension group showed a maximum load of 282 N and total displacement of 6.67 mm. An *in vivo* study of two young adult patients found an average subscapularis contraction of 250 N.⁶ The older demographic considered in the current study may not be able to generate the referenced *in vivo* load.⁶ Osteotomy contact of 23-47% was maintained even with the high total displacements. The failures and total displacement values, however, are still cause for concern. Because these fragments moved an average 6.67 mm after 6 weeks of simulated rehabilitation, osteotomy repairs should be protected during the first 6 weeks.

6.0 CONCLUSIONS AND FUTURE WORK

6.1 CONCLUSION

The study showed that thin osteotomies displaced less than thick osteotomies. This could be due to preservation of humeral bone stock. Adding a tension band improved construct stability and eliminated catastrophic failure modes observed in the compression groups. The ideal repair was a thin wafer with a combination of tension and compression sutures. This construct had the smallest total displacement (6.7mm), osteotomy contact after cyclic loading (37%), and adequate maximum load (282 N). However, these osteotomy repairs still need to be protected during the first six weeks, because the fragment motion after the initial pull and six weeks of simulated rehabilitation is greater than the clinical threshold.

6.2 FUTURE WORK

There were many useful findings in the present study; however, as with most research, there are also many questions that emerged which provide motivation for future work. There are many structural weaknesses observed with these repairs that need to be addressed. Combination of the two most common repair techniques did not significantly decrease the displacements observed compared to previous studies as hoped. This begs the question if the current

configurations are sufficient and perhaps new configurations need to be created to address this issue. Future work could involve creation and testing of these new configurations in an effort to reduce the inherent slack seen in the current systems and produce a distinctly superior repair. One thought inquires if sutures are the answer as a frequent failure mode suture sawing through bone most likely due to stress concentrations. A new repair configuration would have the ability to distribute the loading of the subscapularis more evenly while having, ideally, no slack in the system from which displacement could arise.

The current mechanical analysis would lead one to believe these repairs are insufficient for their purpose. However there are numerous studies reporting clinical success of the lesser tuberosity osteotomy technique. A different direction for future work entails a clinical study comparing the combination with a tension band technique demonstrated superior in this study with the other methods for osteotomy fixation. This study ideally would involve two surgeons, one who performs the tension band technique and the other who performs a compression technique. The clinical study would also include imaging in an attempt to quantify the sizes of the created osteotomies and also images of the shoulder as the patient heals in an attempt to understand the healing process of these repairs in a more detailed manner. Clinical evaluations paired with the images and combined with strength testing of the subscapularis would give the information needed. This strength testing would involve testing the strength of an individual in adduction and internal rotation as these movements isolate the subscapularis muscle. Studies including all of these parameters are ultimately the determining factor for success of the constructs for lesser tuberosity osteotomy fixation.

APPENDIX A

DATA ACQUISITION MATLAB CODE

```
%%% Lesser Tuberosity Study

%%% Reset
close all
clear all

%%% Parameters
fs = 200;
% Sampling Frequency [Hz]
Ts = 1/fs;
% Sampling Period [s]

%%% Data Acquisition Setup
duration = 120;
% Total Acquisition Length [s]
ai = analoginput('mcc');
ch = addchannel(ai,0:5);
% Channels Recorded
set(ai,'SampleRate',fs)
ActualRate = get(ai,'SampleRate');
set(ai,'SamplesPerTrigger',duration*ActualRate)
set(ai,'TriggerChannel',ch(6))
% Trigger Channel
set(ai,'TriggerType','Software')
set(ai,'TriggerCondition','Rising')
set(ai,'TriggerConditionValue',2.5)
% Trigger Level [V]

%%% Acquire Data
start(ai)

%%% Wait Until First Sample Is Saved
while ai.SamplesAvailable==0;
end

%%% Plot Some Data Points During Sampling
```

```

starttime = tic;
counter = 0;
Tp = 0.2;
% Plotting Period [s]

tvec = 0;
yvec = zeros(1,6);

while strcmp(ai.running, 'On')

    deltatime = toc(starttime);

    if deltatime > counter * Tp;
        tvec(counter+1) = Ts * (ai.SamplesAvailable);
        yvec(counter+1, :) = peekdata(ai, 1);

        figure(1)
        plot(tvec, yvec(:, 2), tvec, yvec(:, 6))
        xlabel('Time (s)')
        ylabel('Voltage (V)')
        axis([0 duration -10 10])
        grid on

        counter = counter + 1;
    end
end
wait(ai, inf)

%%% Retrieve and Save Data
[data, t] = getdata(ai);
save static t data
% Save Acquired Data [Filename then Variables]

%%% Figures
figure(2)
plot(t, data(:, 2))
grid on
xlabel('Time (s)')
ylabel('Voltage (V)')

%%% Clean Up Acquisition Object
delete(ai)
clear ai

```

APPENDIX B

DISPLACEMENT COMPUTATIONS MATLAB CODE

```
%This is the overall function to compute the displacements of the
%osteotomies. The program takes in the excel file from the Spica Tech
%tracking system and finds the movement of the osteotomy fragment
compared
%to the humerus. The program then plots all of the data and outputs the
%various displacement calculations. This version of the code includes
the
%osteotomy edge tracking technique identified by OETT.

clear all
close all
clc

Static_Displacement=Displacements('staticOETT.xls');
display('Static Complete');
Min1_Displacement=Displacements('min1_OETT.xls');
display('Minute 1 Complete');
Min49_Displacement=Displacements('min49_OETT.xls');
display('Minute 49 Complete');

oldmarkers=5;
newmarkers=4;

totmarks=oldmarkers+newmarkers;

StaticAvg=Average(Static_Displacement(:,1:oldmarkers));
StaticOETTavg=Average(Static_Displacement(:,(oldmarkers+1):oldmarkers+newmarker
s));
[staticmax,staticspot]=max(StaticAvg);
[staticmax2,staticspot2]=max(StaticOETTavg);

Min1Avg=Average(Min1_Displacement(:,1:oldmarkers));
Min1OETTavg=Average(Min1_Displacement(:,(oldmarkers+1):oldmarkers+newmarkers));
[Min1max,min1spot]=max(Min1Avg);
[Min1max2,min1spot2]=max(Min1OETTavg);
```

```

Min49Avg=Average(Min49_Disp(:,1:oldmarkers));
Min49OETTAvg=Average(Min49_Disp(:,(oldmarkers+1):oldmarkers+newmarkers)
);
[Min49max,min49spot]=max(Min49Avg);
[Min49max2,min49spot2]=max(Min49OETTAvg);

[Cycle1_Orig,loca_Orig]=FirstPeak(Min1Avg);
[Cycle1_OETT,loca_OETT]=FirstPeak(Min1OETTAvg);

[Ampi_Orig,maxi_Orig,mini_Orig]=Amplitudes(Min1Avg);
[Ampi_OETT,maxi_OETT,mini_OETT]=Amplitudes(Min1OETTAvg);

[Ampo_Orig,maxo_Orig,mino_Orig]=Amplitudes(Min49Avg);
[Ampo_OETT,maxo_OETT,mino_OETT]=Amplitudes(Min49OETTAvg);

maxxstatic=max(max(Static_Disp));

if maxxstatic<5
    maxxstatic=5;
else
    maxxstatic=maxxstatic+1;
end

maxxcyclic=max(max(Min49_Disp));
if maxxcyclic<5
    maxxcyclic=5;
else
    maxxcyclic=maxxcyclic+1;
end

[staticsize,rew]=size(Static_Disp);
[Min1size,rew2]=size(Min1_Disp);
[Min49size,rew3]=size(Min49_Disp);

scrsz=get(0,'ScreenSize');
e=figure('Position',[scrsz(1) scrsz(2) scrsz(3) scrsz(4)]);
subplot(2,2,1:2)
cam_time=[0.1:.1:.1*staticsize];

plot(cam_time,StaticAvg,'b','LineWidth',4)
hold on
plot(cam_time,StaticOETTAvg,'r','LineWidth',4)

ylabel('Displacement (mm)')
xlabel('Time (s)')
title('Cycle 1 Displacement')
hold on

plot(cam_time,Static_Disp(:,1),'b','LineWidth',2)
plot(cam_time,Static_Disp(:,2),'g','LineWidth',2)
plot(cam_time,Static_Disp(:,3),'m','LineWidth',2)
plot(cam_time,Static_Disp(:,4),'r','LineWidth',2)
plot(cam_time,Static_Disp(:,5),'c','LineWidth',2)
plot(cam_time,Static_Disp(:,6),'b','LineWidth',2)
plot(cam_time,Static_Disp(:,7),'g','LineWidth',2)

```

```

plot(cam_time,Static_Disp(:,8),'r','LineWidth',2)
plot(cam_time,Static_Disp(:,9),'m','LineWidth',2)

scatter(staticspot/10,staticmax,'b*','LineWidth',3)
scatter(staticspot2/10,staticmax2,'r*','LineWidth',3)
plot([0:.1:staticsize/10],ones(staticsize+1)*5,'k:','LineWidth',2)
legend('Orig Avg','New
Avg','M1','M2','M3','M4','M5','M21','M22','M23','M24','Old Max','New
Max','5mm','Location','southoutside','Orientation','horizontal')
axis([0,staticsize/10,0,maxxstatic])

subplot(2,2,3)
minlcam_time=[0.1:.1:.1*Minlsize];

plot(minlcam_time,MinlAvg,'b:','LineWidth',4)
hold on
plot(minlcam_time,MinlOETTAvg,'r:','LineWidth',4)

ylabel('Displacement (mm)')
xlabel('Time (s)')
title('Cycle 2-6 Displacement')
hold on

plot(minlcam_time,Minl_Disp(:,1),'b','LineWidth',2)
plot(minlcam_time,Minl_Disp(:,2),'g','LineWidth',2)
plot(minlcam_time,Minl_Disp(:,3),'m','LineWidth',2)
plot(minlcam_time,Minl_Disp(:,4),'r','LineWidth',2)
plot(minlcam_time,Minl_Disp(:,5),'c','LineWidth',2)
plot(minlcam_time,Minl_Disp(:,6),'b','LineWidth',2)
plot(minlcam_time,Minl_Disp(:,7),'g','LineWidth',2)
plot(minlcam_time,Minl_Disp(:,8),'r','LineWidth',2)
plot(minlcam_time,Minl_Disp(:,9),'m','LineWidth',2)

scatter(minlspot/10,Minlmax,'b*','LineWidth',3)
scatter(minlspot2/10,Minlmax2,'r*','LineWidth',3)
plot([0:.1:Minlsize/10],ones(Minlsize+1)*5,'k:','LineWidth',2)
scatter(maxi_orig(:,2)/10,maxi_orig(:,1),'ob','LineWidth',2)
scatter(mini_orig(:,2)/10,mini_orig(:,1),'ob','LineWidth',2)
scatter(maxi_OETT(:,2)/10,maxi_OETT(:,1),'or','LineWidth',2)
scatter(mini_OETT(:,2)/10,mini_OETT(:,1),'or','LineWidth',2)
axis([0,Minlsize/10,0,maxxcyclic])

subplot(2,2,4)
min49cam_time=[2995+0.1:.1:.1*Min49size+2995];

plot(min49cam_time,Min49Avg,'b:','LineWidth',4)
hold on
plot(min49cam_time,Min49OETTAvg,'r:','LineWidth',4)

ylabel('Displacement (mm)')
xlabel('Time (s)')
title('Cycle 2996-3000 Displacement')
hold on

plot(min49cam_time,Min49_Disp(:,1),'b','LineWidth',2)

```

```

plot(min49cam_time,Min49_Disp(:,2),'g','LineWidth',2)
plot(min49cam_time,Min49_Disp(:,3),'m','LineWidth',2)
plot(min49cam_time,Min49_Disp(:,4),'r','LineWidth',2)
plot(min49cam_time,Min49_Disp(:,5),'c','LineWidth',2)
plot(min49cam_time,Min49_Disp(:,6),'b','LineWidth',2)
plot(min49cam_time,Min49_Disp(:,7),'g','LineWidth',2)
plot(min49cam_time,Min49_Disp(:,8),'r','LineWidth',2)
plot(min49cam_time,Min49_Disp(:,9),'m','LineWidth',2)
scatter(maxo_orig(:,2)/10+2995,maxo_orig(:,1),'ob','LineWidth',2)
scatter(mino_orig(:,2)/10+2995,mino_orig(:,1),'ob','LineWidth',2)
scatter(maxo_OETT(:,2)/10+2995,maxo_OETT(:,1),'or','LineWidth',2)
scatter(mino_OETT(:,2)/10+2995,mino_OETT(:,1),'or','LineWidth',2)

scatter(min49spot/10+2995,Min49max,'b*','LineWidth',3)
scatter(min49spot2/10+2995,Min49max2,'r*','LineWidth',3)
plot([2995.1:.1:Min49size/10+2995.1],ones(Min49size+1)*5,'k','LineWidt
h',2)
axis([2995,Min49size/10+2995,0,maxxcyclic])

Static_Orig=staticmax
Static_OETT=staticmax2

Minutel_Orig=Minlmax
Minutel_OETT=Minlmax2

Minute49_Orig=Min49max
Minute49_OETT=Min49max2

Cyclic_Elongation_Orig=Minute49_Orig-Cycle1_Orig
Cyclic_Elongation_OETT=Minute49_OETT-Cycle1_OETT

minlCyclic_Amplitude_Orig=Ampi_orig
minlCyclic_Amplitude_OETT=Ampi_OETT

min49Cyclic_Amplitude_Orig=Ampo_orig
min49Cyclic_Amplitude_OETT=Ampo_OETT

Amplitude_Difference_Orig=minlCyclic_Amplitude_Orig-
min49Cyclic_Amplitude_Orig
Amplitude_Difference_OETT=minlCyclic_Amplitude_OETT-
min49Cyclic_Amplitude_OETT

```

```
%%
```

Various Functions called by TuberosityTesting.m

ActuatorUnit.m

```

function [ u ] = ActuatorUnit( filename )
%Takes information about the actuator and outputs the unit vector in
the
%direction of the actuator.

```

```

[actuator_xyz_data,headers]=xlsread(filename);

%size of imported raw data
[c,d]=size(actuator_xyz_data);

k=1;
while k<=(d-2)

    v = genvarname(headers{1,k});
    eval([v ' = actuator_xyz_data(:, k:k+2);']);

    k=k+3;

end

humerus_a=actuator_xyz_data(:,(d-8):d);

ha_1=humerus_a(:,1:3);
ha_2=humerus_a(:,4:6);
ha_3=humerus_a(:,7:9);

%define local coordinate system
r1_a=ha_2-ha_1;
r2_a=ha_3-ha_1;

r3_a=cross(r1_a,r2_a);
r4_a=cross(r3_a,r1_a);

clear v
q=1;

while q<=c

    u1_a=r1_a(q,:)/norm(r1_a(q,:)); % unit vector along new x-axis
    u3_a=r3_a(q,:)/norm(r3_a(q,:)); % unit vector along new z-axis
    u4_a=r4_a(q,:)/norm(r4_a(q,:)); % unit vector along new y-axis

    % u1_a, u3_a, u4_a are orthogonal vectors and represent a
coordinate system

    % Rotation Matrix, R, is then defined as:
    R_act = vertcat(u1_a,u4_a,u3_a).'; % transposed matrix of the 3
orthogonal unit vectors

    a_loc=R_act*[(A1(q,)-ha_1(q,))];

    act_loc(q,1)=a_loc(1,1);
    act_loc(q,2)=a_loc(2,1);
    act_loc(q,3)=a_loc(3,1);

    q=q+1;

```

```
end
```

```
%Now must evaluate movement of markers in the actuator direction
```

```
u=(act_loc(2,:)-act_loc(1,:))/norm(act_loc(2,:)-act_loc(1,:));
```

```
end
```

Amplitudes.m

```
function [Amplitude,maxs,mins] = Amplitudes( signal )
%This function takes in a signal and computes the average amplitude of
the cyclic
%signal. It also returns the locations of each max and min used and
their
%locations.

error=2;
ender=5;

[sigsize,c]=size(signal);

peaks=floor(sigsize/10);

range=2;

maxima=zeros(peaks,2);
location=maxima;
c=0;
d=0;
for b=2:peaks+1
max=-5000;
for a =location(b-1,2)+range:sigsize-range
test=mean(signal(a-range+1:a+range));
if test>max
max=signal(a);
end
test2=mean(signal(a+1:a+range));

if test2<max && abs(max-test2)<error
if signal(a)>signal(a+1) && signal(a)>signal(a-1)
maxima(b,1)=signal(a);
if a<=location(b-1,1)
ender=-43;
break
else
location(b,1)=a;
c=c+1;
break
end
end
end
```

```

        end
    end
    if ender==--43
        break
    else
        min=5000;
        for a =location(b,1)+range:sigsize-range
            test=mean(signal(a-range+1:a+range));
            if test<min
                min=signal(a);
            end

            test2=mean(signal(a+1:a+range));

            if test2>min && abs(min-test2)<error
                if signal(a)<signal(a+1) && signal(a)<signal(a-1)
                    maxima(b,2)=signal(a);
                    if a<=location(b-1,2)
                        ender==--43;
                        break
                    else
                        location(b,2)=a;
                        d=d+1;
                        break
                    end
                end
            end
        end

    end

    if ender==--43
        break
    end
end
end

maxs=zeros(c,2);
mins=zeros(d,2);

for a = 1:c
    maxs(a,1)=maxima(a+1,1);
    maxs(a,2)=location(a+1,1);
end

for a = 1:d
    mins(a,1)=maxima(a+1,2);
    mins(a,2)=location(a+1,2);
end

a=1;
b=1;
ab=1;
Amplist=zeros(c+d-1,1);

if c>d
    while a <=d

```

```

        Amplist(ab)=abs(maxs(a,1)-mins(b,1));
        ab=ab+1;
        a=a+1;
        Amplist(ab)=abs(maxs(a,1)-mins(b,1));
        b=b+1;
        ab=ab+1;
    end
elseif d>c
    while a <=c
        Amplist(ab)=abs(maxs(a,1)-mins(b,1));
        ab=ab+1;
        b=b+1;
        Amplist(ab)=abs(maxs(a,1)-mins(b,1));
        a=a+1;
        ab=ab+1;
    end
else
    while a<c
        Amplist(ab)=abs(maxs(a,1)-mins(b,1));
        ab=ab+1;
        b=b+1;
        Amplist(ab)=abs(maxs(a,1)-mins(b,1));
        a=a+1;
        ab=ab+1;
        Amplist(ab)=abs(maxs(a,1)-mins(b,1));
    end
end
end

```

```
Amplitude=mean(Amplist);
```

```
end
```

Average.m

```

function [ SigAvg ] = Average( signal )
%Takes in a signal and averages the points that are the same to create
an
%average signal.

[signalsize,otherdim]=size(signal);

SigAvg=zeros(signalsize,1);
j=1;

while j<=(signalsize-1)
    SigAvg(j,1)=mean(signal(j,:));
    j=j+1;
end

end

```

Displacements.m

```

function [ M_dir_marker_act ] = Displacements( test )
%This function takes in a set of data and computes the displacements of
the
%markers based on the last three markers (Humerus) in the excel file.

%%
%Import Data and Name

%input name of file
filename=test;
[xyz_data,headers]=xlsread(filename);

%size of imported raw data
[a,b]=size(xyz_data);
num_of_markers=(b-9)/3;
%isolate first column
frame_count=a;

k=1;
while k<=(b-2)

    v = genvarname(headers{1,k});
    eval([v '= xyz_data(:, k:k+2);']);

    k=k+3;
end

humerus_w=xyz_data(:,(b-8):b);
hw_1=humerus_w(:,1:3);
hw_2=humerus_w(:,4:6);
hw_3=humerus_w(:,7:9);

%define local coordinate system
r1=mean(hw_2)-mean(hw_1);
r2=mean(hw_3)-mean(hw_1);

r3=cross(r1,r2);
r4=cross(r3,r1);

p=1;

while p<=a
    u1=r1(1,:)/norm(r1(1,:)); % unit vector along new x-axis
    u3=r3(1,:)/norm(r3(1,:)); % unit vector along new z-axis
    u4=r4(1,:)/norm(r4(1,:)); % unit vector along new y-axis

    % u1, u3, u4 are orthogonal vectors and represent a coordinate system

    % Rotation Matrix, R, is then defined as:
    R_wafer = vertcat(u1,u4,u3)'; % transposed matrix of the 3
orthogonal unit vectors

z=1;

```

```

while z<= num_of_markers

    current_name=horzcat('M',num2str(z));
    m=eval(current_name);

    loc=R_wafer*[(m(p,:)-hw_1(p,:))];

    index=horzcat('m_loc_',num2str(z));
    v = genvarname(index);
    eval([v, '(p,1)=loc(1,1);']);
    eval([v, '(p,2)=loc(2,1);']);
    eval([v, '(p,3)=loc(3,1);']);

    z=z+1;
end
p=p+1;
end

```

```


filename='actuator_movement_1.xls';
[actuator_xyz_data,headers]=xlsread(filename);


[c,d]=size(actuator_xyz_data);

k=1;
while k<=(d-2)

    v = genvarname(headers{1,k});
    eval([v ' = actuator_xyz_data(:, k:k+2);']);

    k=k+3;

end

humerus_a=actuator_xyz_data(:,(d-8):d);

ha_1=humerus_a(:,1:3);
ha_2=humerus_a(:,4:6);
ha_3=humerus_a(:,7:9);


r1_a=ha_2-ha_1;
r2_a=ha_3-ha_1;

r3_a=cross(r1_a,r2_a);
r4_a=cross(r3_a,r1_a);

```

```

clear v
q=1;

while q<=c

    u1_a=r1_a(q,:)/norm(r1_a(q,:)); % unit vector along new x-axis
    u3_a=r3_a(q,:)/norm(r3_a(q,:)); % unit vector along new z-axis
    u4_a=r4_a(q,:)/norm(r4_a(q,:)); % unit vector along new y-axis

    % u1_a, u3_a, u4_a are orthogonal vectors and represent a
coordinate system

    % Rotation Matrix, R, is then defined as:
    R_act = vertcat(u1_a,u4_a,u3_a).'; % transposed matrix of the 3
orthogonal unit vectors

    a_loc=R_act*[(A1(q,)-ha_1(q,))];

    act_loc(q,1)=a_loc(1,1);
    act_loc(q,2)=a_loc(2,1);
    act_loc(q,3)=a_loc(3,1);

    q=q+1;
end

%Now must evaluate movement of markers in the actuator direction

act_dir=(act_loc(2,:)-act_loc(1,:))/norm(act_loc(2,:)-act_loc(1,:));

f=1;
while f<(a)
    h=num_of_markers;
    M_dir_marker_act=0.0;
    for bb=1:h

        if f==1,

M_dir_act(f,bb)=dot((eval(['m_loc_',num2str(bb),'((f+1),:)]))-
eval(['m_loc_',num2str(bb),'(f,:)']),act_dir);

        else

M_dir_act(f,bb)=dot((eval(['m_loc_',num2str(bb),'((f+1),:)]))-
eval(['m_loc_',num2str(bb),'(f,:)']),act_dir)+M_dir_act((f-1),bb);
        end
    end
    f=f+1;
    M_dir_marker_act=M_dir_marker_act+M_dir_act;
end

u=ActuatorUnit('actuator_movement_1.xls');
a=m_locs2('staticredo.xls');

```

```

b=m_locs2(test);
[r,s]=size(a);
j=1;
offset=zeros(r,1);
while j<=r
    offset(j,1)=dot(b(j,:)-a(j,:),u);
j=j+1;
end
total_offset=offset;

for bb=1:h
    M_dir_marker_act(:,bb)=M_dir_marker_act(:,bb)+total_offset(bb);
end

%%

end

```

FirstPeak.m

```

function [maxima,location ] = FirstPeak( signal )
%This function takes in a signal and returns the value and location of
the %first maxima of the signal.

[sigsize,c]=size(signal);

max=-5000;
range=2;
for a = range:sigsize-range
    test=mean(signal(a-range+1:a+range));
    if test>max
        max=signal(a);
    end

    test2=mean(signal(a+1:a+range+1));

    if test2<max
        maxima=max;
        location=a;
        break
    end
end

end

```

m_locs2.m

```

function [MLocs]=m_locs2(filename)

```

```

%Takes in the Excel sheet with the marker tracking data and outputs the
%values adjusted to the local coordinate system.
%Import Data and Name

[xyz_data,headers]=xlsread(filename);

%size of imported raw data
[a,b]=size(xyz_data);
num_of_markers=(b-9)/3;
%isolate first column
frame_count=a;

k=1;
while k<=(b-2)

    v = genvarname(headers{1,k});
    eval([v '= xyz_data(:, k:k+2);']);

    k=k+3;
end

humerus_w=xyz_data(:,(b-8):b);
hw_1=humerus_w(:,1:3);
hw_2=humerus_w(:,4:6);
hw_3=humerus_w(:,7:9);

%define local coordinate system
r1=mean(hw_2)-mean(hw_1);
r2=mean(hw_3)-mean(hw_1);

r3=cross(r1,r2);
r4=cross(r3,r1);

p=1;

while p<=a
    u1=r1(1,:)/norm(r1(1,:)); % unit vector along new x-axis
    u3=r3(1,:)/norm(r3(1,:)); % unit vector along new z-axis
    u4=r4(1,:)/norm(r4(1,:)); % unit vector along new y-axis

    % u1, u3, u4 are orthogonal vectors and represent a coordinate system

    % Rotation Matrix, R, is then defined as:
    R_wafer = vertcat(u1,u4,u3)'; % transposed matrix of the 3
orthogonal unit vectors

z=1;
while z<= num_of_markers

    current_name=horzcat('M',num2str(z));
    m=eval(current_name);

    loc=R_wafer*[(m(p,:)-hw_1(p,:))];

```

```

        index=horzcat('m_loc_',num2str(z));
        v = genvarname(index);
        eval([v, '(p,1)=loc(1,1);']);
        eval([v, '(p,2)=loc(2,1);']);
        eval([v, '(p,3)=loc(3,1);']);

        z=z+1;
    end
    p=p+1;
end

MLocs=zeros(num_of_markers,3);

h=num_of_markers;
for bb=1:h
    MLocs(bb,:)=eval(['m_loc_',num2str(bb),'(1,:)']);
end

```

Offsets.m

```

function [ O ] = Offsets( timepoint )
%This function will give you the offsets for various time points during
the
%experiment.timepoint should be the excel file you want to get the
offsets
%for.

u=ActuatorUnit('actuator_movement_1.xls');

a=m_locs2('staticredo.xls');

b=m_locs2(timepoint);

[r,s]=size(a);

j=1;
offset=zeros(r,1);
while j<=r
    offset(j,1)=dot(b(j,:)-a(j,:),u);
    j=j+1;
end

O=offset;

end

```

sigsearch.m

```
function [ I, sigout ] = sigsearch( sigin, thresh )
%This function takes in a signal and will search in the signal where
the
%signal first reaches a threshold and it will out put a truncated
signal
%starting at that point, it also outputs the index where the truncation
%happened.

[m,n]=size(sigin);

if m>n
    a=m;
elseif m<n
    a=n;
else
    a=1;
    sigout=0;
end

I=1;

for aa=1:a
    if sigin(aa)>=thresh
        break
    else
        I=I+1;
    end
end
b=a-I;
sigout=zeros((b),1);

for aa = 1:b
    sigout(aa)=sigin(aa+I);
end

end
```

APPENDIX C

OSTEOTOMY CONTACT AREA CODE

```
%This program inputs the information generated in the Mimics program to
%estimate the osteotomy contact area after the total displacement. The
%program will ask for an ID of the subject and it will then find the
.stl
%file created in Mimics. The program analyzes the osteotomy fragment
and
%tendon data to compute the area and direction of displacement. The
program
%asks the user at various steps to verify the calculations are correct
and
%offers a manual step to correct any errors. The program then displays
the
%results and computes the percent osteotomy area of overlap after the
%defined displacement.

close all
clear all
clc

ID=input('ID #: ');
Side=input('Side? ', 's');

Tend=stlread([num2str(ID) '/' num2str(ID) Side 'T.stl']);
facestend=Tend.faces;
Xt=Tend.vertices(:,1);
Yt=Tend.vertices(:,2);
Zt=Tend.vertices(:,3);

Ost=stlread([num2str(ID) '/' num2str(ID) Side 'Ost.stl']);
facesost=Ost.faces;
Xo=Ost.vertices(:,1);
Yo=Ost.vertices(:,2);
Zo=Ost.vertices(:,3);

xmax=max(Ost.vertices(:,1));
xmin=min(Ost.vertices(:,1));
```

```

ymax=max(Ost.vertices(:,2));
ymin=min(Ost.vertices(:,2));
zmax=max(Ost.vertices(:,3));
zmin=min(Ost.vertices(:,3));

OPoint=[mean(Ost.vertices(:,1))          mean(Ost.vertices(:,2))
mean(Ost.vertices(:,3))];

Comps=princomp(Ost.vertices);

mag=10;
Prin1=[mean(Ost.vertices(:,1))          mean(Ost.vertices(:,2))
mean(Ost.vertices(:,3));mean(Ost.vertices(:,1))+Comps(1,1)*mag
mean(Ost.vertices(:,2))+Comps(2,1)*mag
mean(Ost.vertices(:,3))+Comps(3,1)*mag];
Prin2=[mean(Ost.vertices(:,1))          mean(Ost.vertices(:,2))
mean(Ost.vertices(:,3));mean(Ost.vertices(:,1))+Comps(1,2)*mag
mean(Ost.vertices(:,2))+Comps(2,2)*mag
mean(Ost.vertices(:,3))+Comps(3,2)*mag];
Prin3=[mean(Ost.vertices(:,1))          mean(Ost.vertices(:,2))
mean(Ost.vertices(:,3));mean(Ost.vertices(:,1))+Comps(1,3)*mag
mean(Ost.vertices(:,2))+Comps(2,3)*mag
mean(Ost.vertices(:,3))+Comps(3,3)*mag];

scrsz=get(0,'ScreenSize');
h=figure('Position',[scrsz(1) scrsz(2) scrsz(3) scrsz(4)]);
trisurf(facestend,Xt,Yt,Zt,'Facecolor','magenta','FaceAlpha',0.35,'Edge
color','none')
hold on
trisurf(facesost,Xo,Yo,Zo,'Facecolor','black','FaceAlpha',0.5,'Edgecolo
r','none')
plot3(Prin1(:,1),Prin1(:,2),Prin1(:,3),'>r-','LineWidth',2)
plot3(Prin2(:,1),Prin2(:,2),Prin2(:,3),'>b-','LineWidth',2)
plot3(Prin3(:,1),Prin3(:,2),Prin3(:,3),'>g-','LineWidth',2)
axis equal
axis vis3d
legend('Subscap          Tendon','LT
Osteotomy','Princomp1','Princomp2','Princomp3')
camlight right;
lighting phong;
xlabel('X-axis')
ylabel('Y-axis')
zlabel('Z-axis')

% pause(10)

Planswer=input('Which component is your normal? ');

close

ONorm=Comps(Planswer,:);

%Project all points onto this plane and allow user to select the area

m=size(Xo,1);

```

```

n=size(Xt,1);
Ostp=ones(m,4);
Tendp=ones(n,4);
Prinlp=ones(2,4);
Prin2p=Prinlp;
Prin3p=Prin2p;

if Planswer == 1
    twond= 2;
else
    twond=1;
end

%Transform data so that the normal is the positive Z axis.

%Create matrices to operate on to determine the Transform

X=[0 0 0; eval(['Prin' num2str(Planswer) '(2,1)'])-OPoint(1)
eval(['Prin' num2str(Planswer) '(2,2)'])-OPoint(2) eval(['Prin'
num2str(Planswer) '(2,3)'])-OPoint(3); eval(['Prin' num2str(twond) '(2,1)'])-
OPoint(1) eval(['Prin' num2str(twond) '(2,2)'])-OPoint(2) eval(['Prin'
num2str(twond) '(2,3)'])-OPoint(3)];
Y=[0 0 0;0 0 mag;mag 0 0];

[R,T,Trans,Err]=rot3dfit(X,Y);

Transform=[R(1,1) R(1,2) R(1,3) T(1);R(2,1) R(2,2) R(2,3) T(2); R(3,1)
R(3,2) R(3,3) T(3); 0 0 0 1];
%Transform

for a = 1:m
    Ostp(a,:)=Transform'*[Ost.vertices(a,1)-OPoint(1)
Ost.vertices(a,2)-OPoint(2) Ost.vertices(a,3)-OPoint(3) 1]';
end

for a = 1:n
    Tendp(a,:)=Transform'*[Tend.vertices(a,1)-OPoint(1)
Tend.vertices(a,2)-OPoint(2) Tend.vertices(a,3)-OPoint(3) 1]';
end

for a = 1:2
    Prinlp(a,:)=Transform'*[Prinl(a,1)-OPoint(1) Prinl(a,2)-OPoint(2)
Prinl(a,3)-OPoint(3) 1]';
    Prin2p(a,:)=Transform'*[Prin2(a,1)-OPoint(1) Prin2(a,2)-OPoint(2)
Prin2(a,3)-OPoint(3) 1]';
    Prin3p(a,:)=Transform'*[Prin3(a,1)-OPoint(1) Prin3(a,2)-OPoint(2)
Prin3(a,3)-OPoint(3) 1]';
end

Tendirs=princomp(Tendp(:,1:3));
TPrinl=[mean(Tendp(:,1)) mean(Tendp(:,2))
mean(Tendp(:,3));mean(Tendp(:,1))+Tendirs(1,1)*mag
mean(Tendp(:,2))+Tendirs(2,1)*mag mean(Tendp(:,3))+Tendirs(3,1)*mag];

```

```

    TPrin2=[mean(Tendp(:,1))                                mean(Tendp(:,2))
mean(Tendp(:,3));mean(Tendp(:,1))+Tendirs(1,2)*mag
mean(Tendp(:,2))+Tendirs(2,2)*mag mean(Tendp(:,3))+Tendirs(3,2)*mag];
    TPrin3=[mean(Tendp(:,1))                                mean(Tendp(:,2))
mean(Tendp(:,3));mean(Tendp(:,1))+Tendirs(1,3)*mag
mean(Tendp(:,2))+Tendirs(2,3)*mag mean(Tendp(:,3))+Tendirs(3,3)*mag];

    scrsz=get(0,'ScreenSize');
    h=figure('Position',[scrsz(1) scrsz(2) scrsz(3) scrsz(4)]);

    subplot(1,2,1)

    trisurf(facestend,Tendp(:,1),Tendp(:,2),Tendp(:,3),'Facecolor','magenta
','FaceAlpha',0.35,'Edgecolor','none')
    hold on
    trisurf(facesost,Ostp(:,1),Ostp(:,2),Ostp(:,3),'Facecolor','black','Fac
eAlpha',0.5,'Edgecolor','none')
    plot3(Prin1p(:,1),Prin1p(:,2),Prin1p(:,3),'>r-', 'LineWidth',2)
    plot3(Prin2p(:,1),Prin2p(:,2),Prin2p(:,3),'>b-', 'LineWidth',2)
    plot3(Prin3p(:,1),Prin3p(:,2),Prin3p(:,3),'>g-', 'LineWidth',2)
    plot3(TPrin1(:,1),TPrin1(:,2),TPrin1(:,3),'>c-', 'LineWidth',2)
    plot3(TPrin2(:,1),TPrin2(:,2),TPrin2(:,3),'>y-', 'LineWidth',2)
    plot3(TPrin3(:,1),TPrin3(:,2),TPrin3(:,3),'>k-', 'LineWidth',2)
    axis equal
    axis vis3d
    legend('Subscap Tendon','LT Osteotomy','OstDir-1','OstDir-2','OstDir-
3','TDir-1','TDir-2','TDir-3')
    camlight right;
    lighting phong;
    xlabel('X Axis')
    ylabel('Y Axis')
    zlabel('Z Axis')

    % pause(10)

    Planswer2=input('Which component is your normal? ');

    Tdir=Tendirs(:,Planswer2);

    %Show projection of osteotomy area with the tendon direction vector

    OA=Ostp(:,1:2);
    Tvec=Tdir(1:2)/sqrt(Tdir(1)^2+Tdir(2)^2);
    Tvecs=zeros(mag,2);
    for a = 2:mag
        Tvecs(a,:)=[Tvec(1)*(a-1) Tvec(2)*(a-1)];
    end

    subplot(1,2,2)

    scatter(OA(:,1),OA(:,2),'.k','LineWidth',2)

```

```

hold on
plot(Tvecs(:,1),Tvecs(:,2),'>m-', 'LineWidth',2)
legend('LT Ost Area', 'Tendon Direction')
xlabel('X axis')
ylabel('Y axis')
axis equal
grid on

a=1;

while a<2
    Planswer3=input('Tendon Direction Correct? (y/n/r) :','s');
    if Planswer3=='n'
        Tvecs=-1*Tvecs;
        Tvec=-1*Tvec;
        cla

        subplot(1,2,2)

        scatter(OA(:,1),OA(:,2),'.k', 'LineWidth',2)
        hold on
        plot(Tvecs(:,1),Tvecs(:,2),'>m-', 'LineWidth',2)
        legend('LT Ost Area', 'Tendon Direction')
        xlabel('X axis')
        ylabel('Y axis')
        axis equal
        grid on
    elseif Planswer3 == 'r'
        close
        scrsz=get(0, 'ScreenSize');
        figure('Position',[scrsz(1) scrsz(2) scrsz(3) scrsz(4)]);
        scatter(OA(:,1),OA(:,2),'.k', 'LineWidth',2)
        hold on
        scatter(Tendp(:,1),Tendp(:,2),'.m', 'LineWidth',2)
        axis equal
        grid on
        xlabel('X axis')
        ylabel('Y axis')
        title('Define Tendon Vector')
        [xt,yt]=ginput(2);

        Tvec=[xt(2)-xt(1)      yt(2)-yt(1)]/sqrt((xt(2)-xt(1))^2+(yt(2)-
yt(1))^2);
        Tvecs=zeros(mag,2);
        for a = 2:mag
            Tvecs(a,:)=[Tvec(1)*(a-1) Tvec(2)*(a-1)];
        end

        plot(Tvecs(:,1),Tvecs(:,2),'>m-', 'LineWidth',2)
        legend('LT Ost Area', 'Tendon Direction')

        Planswer35=input('Direction good? (y/n) :','s');

        if Planswer35 == 'n'

```

```

        Tvec=(-1)*Tvec;
        Tvecs=(-1)*Tvecs;
        a=2;
        close
    else
        a=2;
        close
    end
else
    a=2;
    close
end

end

pxscale=10;
Omaxx=ceil(max(OA(:,1))-min(OA(:,1)))*pxscale;
Omaxy=ceil(max(OA(:,2))-min(OA(:,2)))*pxscale;
buffer=20;

OAt=OA;
Tvecst=Tvecs;
OAI=zeros(Omaxy+buffer,Omaxx+buffer,'uint8');

for a = 1:m
    OAt(a,1)=round(OA(a,1)*pxscale+abs((min(OA(:,1))-1)*pxscale))-
pxscale+buffer/2;
    OAt(a,2)=-round(OA(a,2)*pxscale-abs((max(OA(:,2))+1)*pxscale)-
pxscale+buffer/2;
    OAI(OAt(a,2),OAt(a,1))=255;
end

for a = 1:mag
    Tvecst(a,1)=round(Tvecs(a,1)*pxscale+abs((min(OA(:,1))-
1)*pxscale))-pxscale+buffer/2;
    Tvecst(a,2)=-round(Tvecs(a,2)*pxscale-
abs((max(OA(:,2))+1)*pxscale)-pxscale+buffer/2;
    if Tvecst(a,1) <= Omaxx && Tvecst(a,2) <= Omaxy && Tvecst(a,1)>0 &&
Tvecst(a,2) > 0
        OAI(Tvecst(a,2),Tvecst(a,1))=100;
    end
end

[BW,xi,yi] = roipoly2(OAI);

close

Ost.area=polygeom( xi/10, yi/10 );

oxi=xi/10-Ost.area(2);
oyi=-(yi/10-Ost.area(3));

Planswer4=input('What was the total displacement? ');
oxf=oxi+Planswer4*Tvec(1);
oyf=oyi+Planswer4*Tvec(2);

```

```

[ocx,ocy]=polybool('intersection',oxi,oyi,oxf,oyf);

if size(ocx,1) > 0
    Ost.contactarea=polygeom(ocx, ocy);

    POC=(Ost.contactarea(1)/Ost.area(1))*100;

    scrsz=get(0,'ScreenSize');
    figure('Position',[scrsz(1) scrsz(2) scrsz(3) scrsz(4)]);
    plot(oxi,oyi,'k-', 'LineWidth',3)
    hold on
    xlabel('X axis (mm)')
    ylabel('Y axis (mm)')
    axis equal
    grid on
    plot(oxf,oyf,'b-', 'LineWidth',3)
    patch(ocx,ocy,1,'FaceColor','r')
    plot(ocx,ocy,'k--', 'LineWidth',3)
    plot(Tvecs(:,1),Tvecs(:,2),'g:', 'LineWidth',3)
    legend('Original Osteotomy Area','Displaced Osteotomy
Area','Osteotomy Contact Area','Contact Outline','Tendon Direction Vector')
    title(['ID: ', num2str(ID), ' ', Side,', Osteotomy Area: ',
num2str(Ost.area(1)), ' mm^2 Total Displacement: ', num2str(Planswer4), ' mm
Osteotomy Contact Area: ', num2str(Ost.contactarea(1)), ' mm^2 Percent
Osteotomy Contact: ', num2str(POC),' %'])
else
    Ost.contactarea=0;
    POC=0;
    scrsz=get(0,'ScreenSize');
    figure('Position',[scrsz(1) scrsz(2) scrsz(3) scrsz(4)]);
    plot(oxi,oyi,'k-', 'LineWidth',3)
    hold on
    xlabel('X axis (mm)')
    ylabel('Y axis (mm)')
    axis equal
    grid on
    plot(oxf,oyf,'b-', 'LineWidth',3)
    plot(Tvecs(:,1),Tvecs(:,2),'g:', 'LineWidth',3)
    legend('Original Osteotomy Area','Displaced Osteotomy Area','Tendon
Direction Vector')
    title(['ID: ', num2str(ID), ' ', Side,', Osteotomy Area: ',
num2str(Ost.area(1)), ' mm^2 Total Displacement: ', num2str(Planswer4), ' mm
Osteotomy Contact Area: ', num2str(Ost.contactarea(1)), ' mm^2 Percent
Osteotomy Contact: ', num2str(POC),' %'])
end
end

```

The following m-files are called while running the above program:

polygeom.m

```

function [ geom, iner, cpmo ] = polygeom( x, y )
%POLYGEOM Geometry of a planar polygon
%

```

```

% POLYGEOM( X, Y ) returns area, X centroid,
% Y centroid and perimeter for the planar polygon
% specified by vertices in vectors X and Y.
%
% [ GEOM, INER, CPMO ] = POLYGEOM( X, Y ) returns
% area, centroid, perimeter and area moments of
% inertia for the polygon.
% GEOM = [ area  X_cen  Y_cen  perimeter ]
% INER = [ Ixx  Iyy  Ixy  Iuu  Ivv  Iuv ]
% u,v are centroidal axes parallel to x,y axes.
% CPMO = [ I1  angl  I2  ang2  J ]
% I1,I2 are centroidal principal moments about axes
% at angles angl,ang2.
% angl and ang2 are in radians.
% J is centroidal polar moment.  J = I1 + I2 = Iuu + Ivv

% H.J. Sommer III - 02.05.14 - tested under MATLAB v5.2
%
% sample data
% x = [ 2.000  0.500  4.830  6.330 ]';
% y = [ 4.000  6.598  9.098  6.500 ]';
% 3x5 test rectangle with long axis at 30 degrees
% area=15, x_cen=3.415, y_cen=6.549, perimeter=16
% Ixx=659.561, Iyy=201.173, Ixy=344.117
% Iuu=16.249, Ivv=26.247, Iuv=8.660
% I1=11.249, angl=30deg, I2=31.247, ang2=120deg, J=42.496
%
% H.J. Sommer III, Ph.D., Professor of Mechanical Engineering, 337
Leonhard Bldg
% The Pennsylvania State University, University Park, PA 16802
% (814)863-8997 FAX (814)865-9693 hjs1@psu.edu
www.me.psu.edu/sommer/

% begin function POLYGEOM

% check if inputs are same size
if ~isequal( size(x), size(y) ),
    error( 'X and Y must be the same size' );
end

% number of vertices
[ x, ns ] = shiftdim( x );
[ y, ns ] = shiftdim( y );
[ n, c ] = size( x );

% temporarily shift data to mean of vertices for improved accuracy
xm = mean(x);
ym = mean(y);
x = x - xm*ones(n,1);
y = y - ym*ones(n,1);

% delta x and delta y
dx = x( [ 2:n 1 ] ) - x;
dy = y( [ 2:n 1 ] ) - y;

```

```

% summations for CW boundary integrals
A = sum( y.*dx - x.*dy )/2;
Axc = sum( 6*x.*y.*dx -3*x.*x.*dy +3*y.*dx.*dx +dx.*dx.*dy )/12;
Ayc = sum( 3*y.*y.*dx -6*x.*y.*dy -3*x.*dy.*dy -dx.*dy.*dy )/12;
Ixx = sum( 2*y.*y.*y.*dx -6*x.*y.*y.*dy -6*x.*y.*dy.*dy ...
          -2*x.*dy.*dy.*dy -2*y.*dx.*dy.*dy -dx.*dy.*dy.*dy )/12;
Iyy = sum( 6*x.*x.*y.*dx -2*x.*x.*x.*dy +6*x.*y.*dx.*dx ...
          +2*y.*dx.*dx.*dx +2*x.*dx.*dx.*dy +dx.*dx.*dx.*dy )/12;
Ixy = sum( 6*x.*y.*y.*dx -6*x.*x.*y.*dy +3*y.*y.*dx.*dx ...
          -3*x.*x.*dy.*dy +2*y.*dx.*dx.*dy -2*x.*dx.*dy.*dy )/24;
P = sum( sqrt( dx.*dx +dy.*dy ) );

% check for CCW versus CW boundary
if A < 0,
    A = -A;
    Axc = -Axc;
    Ayc = -Ayc;
    Ixx = -Ixx;
    Iyy = -Iyy;
    Ixy = -Ixy;
end

% centroidal moments
xc = Axc / A;
yc = Ayc / A;
Iuu = Ixx - A*yc*yc;
Ivv = Iyy - A*xc*xc;
Iuv = Ixy - A*xc*yc;
J = Iuu + Ivv;

% replace mean of vertices
x_cen = xc + xm;
y_cen = yc + ym;
Ixx = Iuu + A*y_cen*y_cen;
Iyy = Ivv + A*x_cen*x_cen;
Ixy = Iuv + A*x_cen*y_cen;

% principal moments and orientation
I = [ Iuu -Iuv ;
      -Iuv Ivv ];
[ eig_vec, eig_val ] = eig(I);
I1 = eig_val(1,1);
I2 = eig_val(2,2);
ang1 = atan2( eig_vec(2,1), eig_vec(1,1) );
ang2 = atan2( eig_vec(2,2), eig_vec(1,2) );

% return values
geom = [ A x_cen y_cen P ];
iner = [ Ixx Iyy Ixy Iuu Ivv Iuv ];
cpmo = [ I1 ang1 I2 ang2 J ];

% end of function POLYGEOM

```

rot3dfit.m

```

function [R,T,Yf,Err] = rot3dfit(X,Y)
%ROT3DFIT Determine least-square rigid rotation and translation.
% [R,T,Yf] = ROT3DFIT(X,Y) permforms a least-square fit for the
% linear form
%
% Y = X*R + T
%
% where R is a 3 x 3 orthogonal rotation matrix, T is a 1 x 3
% translation vector, and X and Y are 3D points sets defined as
% N x 3 matrices. Yf is the best-fit matrix.
%
% See also SVD, NORM.
%
% rot3dfit: Frank Evans, NHLBI/NIH, 30 November 2001
%
% ROT3DFIT uses the method described by K. S. Arun, T. S. Huang, and
% S. D. Blostein, "Least-Squares Fitting of Two 3-D Point Sets",
% IEEE Transactions on Pattern Analysis and Machine Intelligence,
% PAMI-9(5): 698 - 700, 1987.
%
% A better theoretical development is found in B. K. P. Horn,
% H. M. Hilden, and S. Negahdaripour, "Closed-form solution of
% absolute orientation using orthonormal matrices", Journal of the
% Optical Society of America A, 5(7): 1127 - 1135, 1988.
%
% Special cases, e.g. colinear and coplanar points, are not
% implemented.

    error(nargchk(2,2,nargin));
    if size(X,2) ~= 3, error('X must be N x 3'); end;
    if size(Y,2) ~= 3, error('Y must be N x 3'); end;
    if size(X,1) ~= size(Y,1), error('X and Y must be the same size');
end;

% mean correct

Xm = mean(X,1); X1 = X - ones(size(X,1),1)*Xm;
Ym = mean(Y,1); Y1 = Y - ones(size(Y,1),1)*Ym;

% calculate best rotation using algorithm 12.4.1 from
% G. H. Golub and C. F. van Loan, "Matrix Computations"
% 2nd Edition, Baltimore: Johns Hopkins, 1989, p. 582.

XtY = (X1')*Y1;
[U,S,V] = svd(XtY);
R = U*(V');

% solve for the translation vector

T = Ym - Xm*R;

% calculate fit points

Yf = X*R + ones(size(X,1),1)*T;

```

```

% calculate the error

dY = Y - Yf;
Err = norm(dY, 'fro'); % must use Frobenius norm

```

stlread.m

```

function varargout = stlread(file)
% STLREAD imports geometry from an STL file into MATLAB.
%     FV = STLREAD(FILENAME) imports triangular faces from the ASCII or
binary
with fields
%     STL file idicated by FILENAME, and returns the patch struct FV,
%     'faces' and 'vertices'.
%
%     [F,V] = STLREAD(FILENAME) returns the faces F and vertices V
separately.
%
%     [F,V,N] = STLREAD(FILENAME) also returns the face normal vectors.
%
%     The faces and vertices are arranged in the format used by the
PATCH plot
%     object.

% Copyright 2011 The MathWorks, Inc.

if ~exist(file,'file')
    error(['File ''%s'' not found. If the file is not on MATLAB''s
path' ...
        ', be sure to specify the full path to the file.'],
file);
end

fid = fopen(file,'r');
if ~isempty(ferror(fid))
    error(lasterror); %#ok
end

M = fread(fid,inf,'uint8=>uint8');
fclose(fid);

[f,v,n] = stlbinary(M);
%if( isbinary(M) ) % This may not be a reliable test
%     [f,v,n] = stlbinary(M);
%else
%     [f,v,n] = stlascii(M);
%end

varargout = cell(1,nargout);
switch nargout
    case 2
        varargout{1} = f;

```

```

        varargout{2} = v;
    case 3
        varargout{1} = f;
        varargout{2} = v;
        varargout{3} = n;
    otherwise
        varargout{1} = struct('faces',f,'vertices',v);
    end
end

function [F,V,N] = stlbinary(M)

F = [];
V = [];
N = [];

if length(M) < 84
    error('MATLAB:stlread:incorrectFormat', ...
        'Incomplete header information in binary STL file.');
```

of faces

```

end

% Bytes 81-84 are an unsigned 32-bit integer specifying the number
% that follow.
numFaces = typecast(M(81:84),'uint32');
%numFaces = double(numFaces);
if numFaces == 0
    warning('MATLAB:stlread:nodata','No data in STL file.');
```

vector

```

    return
end

T = M(85:end);
F = NaN(numFaces,3);
V = NaN(3*numFaces,3);
N = NaN(numFaces,3);

numRead = 0;
while numRead < numFaces
    % Each facet is 50 bytes
    % - Three single precision values specifying the face normal
    % - Three single precision values specifying the first vertex
    (XYZ)
    % - Three single precision values specifying the second vertex
    (XYZ)
    % - Three single precision values specifying the third vertex
    (XYZ)
    % - Two unused bytes
    i1 = 50 * numRead + 1;
    i2 = i1 + 50 - 1;
    facet = T(i1:i2)';

    n = typecast(facet(1:12),'single');
```

```

v1 = typecast(facet(13:24),'single');
v2 = typecast(facet(25:36),'single');
v3 = typecast(facet(37:48),'single');

n = double(n);
v = double([v1; v2; v3]);

% Figure out where to fit these new vertices, and the face, in
the
% larger F and V collections.
fInd = numRead + 1;
vInd1 = 3 * (fInd - 1) + 1;
vInd2 = vInd1 + 3 - 1;

V(vInd1:vInd2,:) = v;
F(fInd,:) = vInd1:vInd2;
N(fInd,:) = n;

numRead = numRead + 1;
end

end

function [F,V,N] = stlascii(M)
warning('MATLAB:stlread:ascii','ASCII STL files currently not
supported.');
```

F = [];

V = [];

N = [];

```

end

% TODO: Change the testing criteria! Some binary STL files still begin
with
% 'solid'.
function tf = isbinary(A)
% ISBINARY uses the first line of an STL file to identify its format.
if isempty(A) || length(A) < 5
error('MATLAB:stlread:incorrectFormat', ...
'File does not appear to be an ASCII or binary STL
file.');
```

end

```

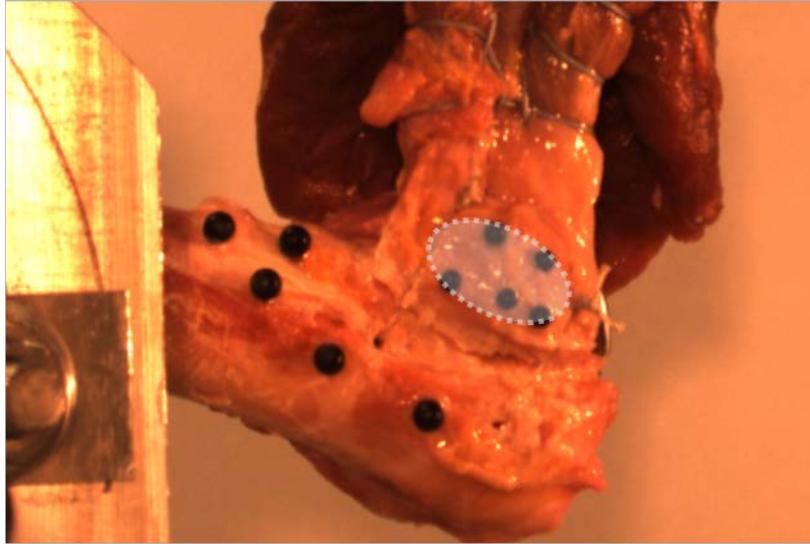
if strcmpi('solid',char(A(1:5)))
tf = false; % ASCII
else
tf = true; % Binary
end
end
end

```

APPENDIX D

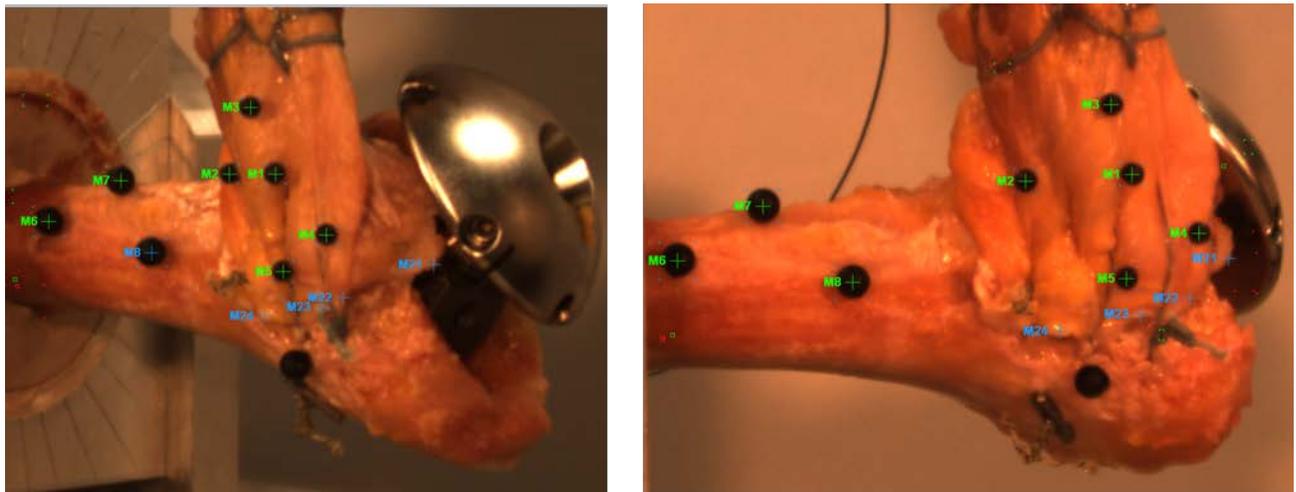
OSTEOTOMY EDGE TRACKING TECHNIQUE

Using the area calculation from the CT scans the osteotomy fragment size was estimated for each specimen. This area was overlapped onto the osteotomy site and it was determined if the markers were placed on the osteotomy fragment or onto the tendon. If the markers were outside of this region their displacement values were deemed questionable as part of the displacement could occur due to tendon stretching. The two figures below illustrate one example where all the markers fall within the region while the second picture has some markers outside of the region. 7 out of the 24 specimens had markers lying outside of the region.

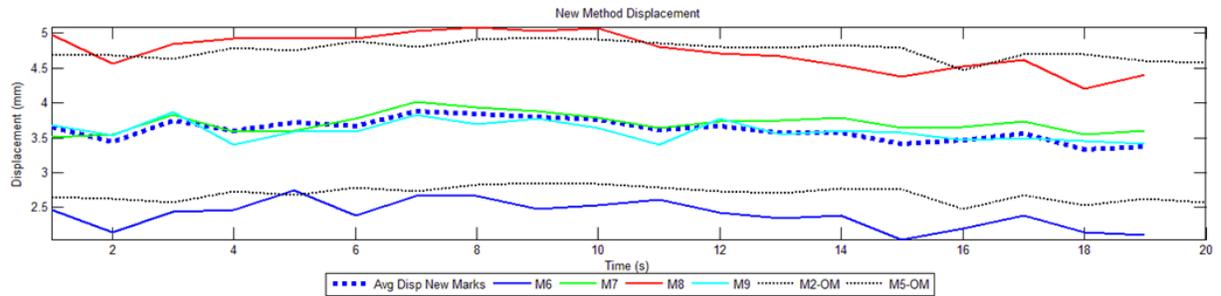
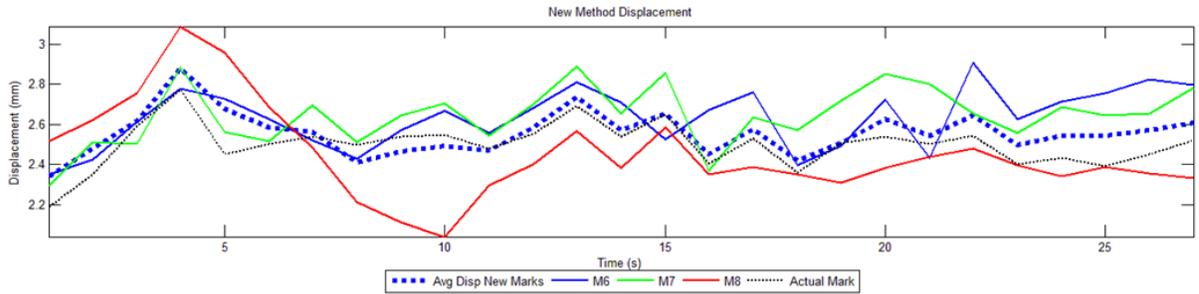


The effects of this on the data was unknown, but it was determined that using the markers outside of the acceptable regions would create questionable data. In an attempt to not bias the results by simply choosing “good” and “bad” markers it was determined that a new method of tracking should be attempted to obtain the results. This method identifies landmarks on the osteotomy edge that are visible in both camera angles and throughout the experiment. Each

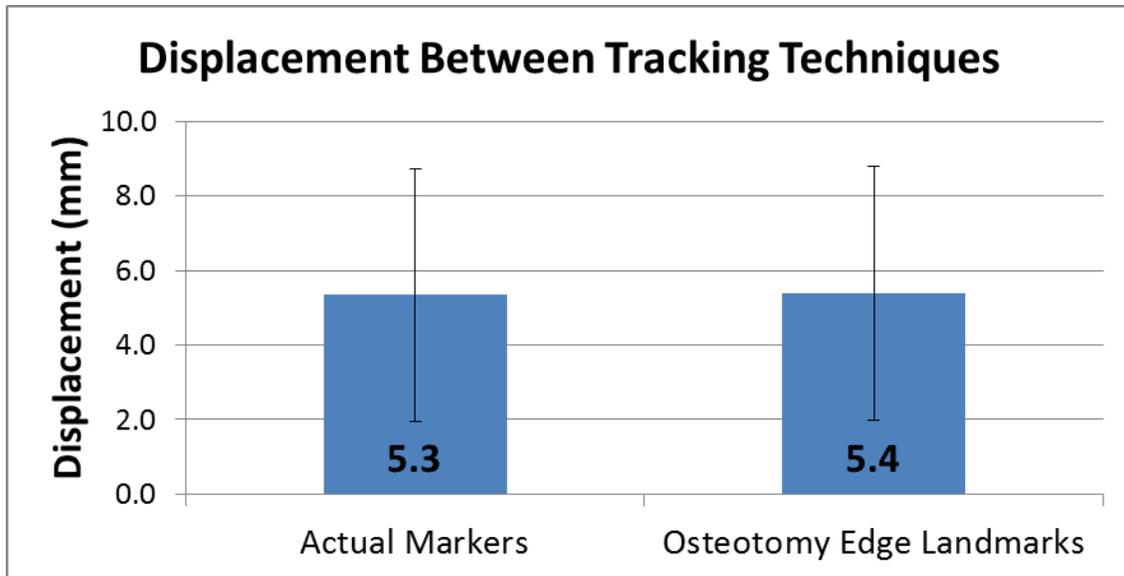
landmark was manually tracked frame by frame to obtain displacement values. An example of markers along the osteotomy edge as well as the original markers is shown below for each camera angle. The original markers are in green and the new markers along the osteotomy edge are in blue.



The contrast to determine landmarks was not the greatest; this is why black markers were chosen in the first place. However this procedure was completed for all specimens and displacement values were computed for the first cycle of the experiment to verify if the new displacement values were accurate and repeatable. For validation, comparison to markers that were within the estimated area region discussed above were used. The following plots show the new technique compared to actual acceptable marker displacements. The actual markers are black dotted lines.



As you can see the new method markers are similar to the actual markers and this relationship was seen for all specimens. Ultimately all specimens were re-tracked with this method and the average initial displacement was compared between the two methods, the initial method again only included markers within the acceptable region for comparison. Below is a bar plot displaying the results.



As you can see the displacement values came out to be very similar. There was a paired students t-test performed to detect differences and none were detected ($p = 0.82$). The difference between the groups was 0.1 mm which is far less than the standard deviation of the specimens themselves (± 3.61 mm). The new tracking technique was deemed reliable and was performed on every test for every specimen to verify the displacements were the most appropriate.

BIBLIOGRAPHY

1. AAOS 2011 Shoulder Joint Replacement <http://orthoinfo.aaos.org/topic.cfm?topic=A00094>
2. Ahmad CS, Wing D, Gardner TR, Levine WN and Bigliani LU. Biomechanical evaluation of subscapularis repair used during shoulder arthroplasty. *J Shoulder Elbow Surg* 2007;16:S59-64. doi: 10.1016/j.jse.2006.09.002
3. Angela E. Kedgley GAM, Louis M. Ferreira, James A. Johnson, Kenneth J. Faber. In vitro kinematics of the shoulder following rotator cuff injury. *Clinical Biomechanics* 2007;22: 1068–1073. doi:
4. Björn Marquardt M, a Stefan Garmann, Christof Hurschler, Wolfgang Pözl, Wolfram Steens, Kai-Axel Witt, Jorn Steinbeck. The influence of arthroscopic subscapularis tendon and anterior capsular release on glenohumeral translation: A biomechanical model. *Journal of Shoulder and Elbow Surgery* 2006;15: 502-508. doi:
5. Bohsali KI, Wirth MA and Rockwood CA, Jr. Complications of total shoulder arthroplasty. *J Bone Joint Surg Am* 2006;88:2279-92. doi: 10.2106/JBJS.F.00125
6. Bull AM, Reilly P, Wallace AL, Amis AA and Emery RJ. A novel technique to measure active tendon forces: application to the subscapularis tendon. *Knee Surg Sports Traumatol Arthrosc* 2005;13:145-50. doi: 10.1007/s00167-004-0556-y
7. David C. Ackland MGP. Lines of action and stabilizing potential of the shoulder. *J Anat* 2009;215: 184-197. doi:
8. David C. Ackland PP, Martin Richardson, Marcus G. Pandy. Moment arms of the muscles crossing the anatomical shoulder. *J Anat* 2008;213: 383-390. doi:
9. DeVries NA, Gassman EE, Kallemeyn NA, Shivanna KH, Magnotta VA and Grosland NM. Validation of phalanx bone three-dimensional surface segmentation from computed tomography images using laser scanning. *Skeletal Radiol* 2008;37:35-42. doi: 10.1007/s00256-007-0386-3
10. Eiji Itoi SRN, David K. Kuechle, Bernard F. Morrey, Kai-Nan An. Dynamic Anterior Stabilizers of the Shoulder with The Arm in Abduction. *Journal of Bone Joint Surgery* 1994;76: 834-836. doi:
11. Genant HK, Engelke K and Prevrhal S. Advanced CT bone imaging in osteoporosis. *Rheumatology (Oxford)* 2008;47 Suppl 4:iv9-16. doi: 10.1093/rheumatology/ken180

12. Geoffrey S. Van Thiel VMW, Fan-Chia Wang, Shane J. Nho, Dana P. Piasecki, Mernard R. Bach Jr., Anthony A. Romeo. Biomechanical similarities among subscapularis repairs after total shoulder arthroplasty. *Journal of Shoulder and Elbow Surgery* 2010;19: 657-663. doi:
13. Gerber C, Yian EH, Pfirrmann CA, Zumstein MA and Werner CM. Subscapularis muscle function and structure after total shoulder replacement with lesser tuberosity osteotomy and repair. *J Bone Joint Surg Am* 2005;87:1739-45. doi: 10.2106/JBJS.D.02788
14. Gerber C, Pennington SD, Yian EH, Pfirrmann CA, Werner CM and Zumstein MA. Lesser tuberosity osteotomy for total shoulder arthroplasty. Surgical technique. *J Bone Joint Surg Am* 2006;88 Suppl 1 Pt 2:170-7. doi: 10.2106/JBJS.F.00407
15. Giuseffi SA, Wongtriratanachai P, Omae H, Cil A, Zobitz ME, An KN, Sperling JW and Steinmann SP. Biomechanical comparison of lesser tuberosity osteotomy versus subscapularis tenotomy in total shoulder arthroplasty. *J Shoulder Elbow Surg* 2012;21:1087-95. doi: 10.1016/j.jse.2011.07.008
16. Glenn C. Terry M and Thomas M. Chopp M. Functional Anatomy of the Shoulder. *Journal of Athletic Training* 2000;35(3):248-255. doi:
17. Gonzalez RC and Woods RE. Image Segmentation. M. McDonald. *Digital Image Processing*.2008. 689-785
18. Heckman DS, Hoover SA, Weinhold PS, Spang JT and Creighton RA. Repair of lesser tuberosity osteotomy for shoulder arthroplasty: biomechanical evaluation of the Backpack and Dual Row techniques. *J Shoulder Elbow Surg* 2011;20:491-6. doi: 10.1016/j.jse.2010.08.004
19. Hudak PL, Amadio PC and Bombardier C. Development of an upper extremity outcome measure: the DASH (disabilities of the arm, shoulder and hand) [corrected]. The Upper Extremity Collaborative Group (UECG). *Am J Ind Med* 1996;29:602-8. doi: 10.1002/(SICI)1097-0274(199606)29:6<602::AID-AJIM4>3.0.CO;2-L
20. Huiskes R and Rietbergen B. Biomechanics of Bone. V. C. Mow. *Basic Orthopaedic Biomechanics and Mechano-Biology*.2005. 123-180
21. Jackson JD, Cil A, Smith J and Steinmann SP. Integrity and function of the subscapularis after total shoulder arthroplasty. *J Shoulder Elbow Surg* 2010;19:1085-90. doi: 10.1016/j.jse.2010.04.001
22. Jandhyala S, Unnithan A, Hughes S and Hong T. Subscapularis tenotomy versus lesser tuberosity osteotomy during total shoulder replacement: a comparison of patient outcomes. *J Shoulder Elbow Surg* 2011;20:1102-7. doi: 10.1016/j.jse.2011.03.019
23. Krishnan SG, Stewart DG, Reineck JR, Lin KC, Buzzell JE and Burkhead WZ. Subscapularis repair after shoulder arthroplasty: biomechanical and clinical validation of a novel technique. *J Shoulder Elbow Surg* 2009;18:184-92; discussion 197-8. doi: 10.1016/j.jse.2008.09.009

24. Michael J. DeFranco LDH, Jon J. P. Warner. Subscapularis Management in Open Shoulder Surgery. *Journal of American Academy of Orthopedic Surgery* 2010;18: 707-717. doi:
25. Miller BS, Joseph TA, Noonan TJ, Horan MP and Hawkins RJ. Rupture of the subscapularis tendon after shoulder arthroplasty: diagnosis, treatment, and outcome. *J Shoulder Elbow Surg* 2005;14:492-6. doi: 10.1016/j.jse.2005.02.013
26. Miller SL, Hazrati Y, Klepps S, Chiang A and Flatow EL. Loss of subscapularis function after total shoulder replacement: A seldom recognized problem. *J Shoulder Elbow Surg* 2003;12:29-34. doi: 10.1067/mse.2003.128195
27. Moeckel BH, Altchek DW, Warren RF, Wickiewicz TL and Dines DM. Instability of the shoulder after arthroplasty. *J Bone Joint Surg Am* 1993;75:492-7. doi:
28. N. Wuelker CJWh, W. Plitz and B. Roetman. A Dynamic Shoulder Model: Reliability Testing and Muscle Force Study. *J Biomech* 1995;28: 489-499. doi:
29. Neter J, Kutner MH, Nachtsheim CJ and Wasserman W. *Applied Linear Statistical Models*. WCB/McGraw-Hill; 1996. p:1186. (ISBN No. 0256024472)
30. Netter FH. *Atlas of Human Anatomy 5th Edition*. Philadelphia, PA: Saunders Elsevier; 2011. (ISBN No.
31. Peter Reilly AMJb, Andrew A. Amis, Andrew L. Wallace, Roger J. H. Emery. Arthroscopically Insertable Force Probes in the Rotator Cuff In Vivo. *Arthroscopy: The Journal of Arthroscopic and Related Surgery* 2003;19: 1-3. doi:
32. Ponce BA, Ahluwalia RS, Mazzocca AD, Gobezie RG, Warner JJ and Millett PJ. Biomechanical and clinical evaluation of a novel lesser tuberosity repair technique in total shoulder arthroplasty. *J Bone Joint Surg Am* 2005;87 Suppl 2:1-8. doi: 10.2106/JBJS.E.00441
33. Prince JL and Links JM. Computed Tomography. *Medical Imaging Signals and Systems*.2006. 181-208
34. Qureshi S, Hsiao A, Klug RA, Lee E, Braman J and Flatow EL. Subscapularis function after total shoulder replacement: results with lesser tuberosity osteotomy. *J Shoulder Elbow Surg* 2008;17:68-72. doi: 10.1016/j.jse.2007.04.018
35. Rathnayaka K, Sahama T, Schuetz MA and Schmutz B. Effects of CT image segmentation methods on the accuracy of long bone 3D reconstructions. *Med Eng Phys* 2011;33:226-33. doi: 10.1016/j.medengphy.2010.10.002
36. Rei Omi HS, Masahiro Ohnuma, Koshi N. Kishimoto, Shoichi Watabuki, Manabu Tashiro, Eiji Itoi. Function of the shoulder muscles during arm elevation: an assessment using positron emission tomography. *J Anat* 2010;216: 643-649. doi:
37. Richard E. Hughes P and and Kai-Nan An P. Force Analysis of Rotator Cuff Muscles. *Clin Orthop Relat Res* 1996;330: 75-83. doi:

38. Scalise JJ, Ciccone J and Iannotti JP. Clinical, radiographic, and ultrasonographic comparison of subscapularis tenotomy and lesser tuberosity osteotomy for total shoulder arthroplasty. *J Bone Joint Surg Am* 2010;92:1627-34. doi: 10.2106/JBJS.G.01461
39. Tingart MJ, Apreleva M, von Stechow D, Zurakowski D and Warner JJ. The cortical thickness of the proximal humeral diaphysis predicts bone mineral density of the proximal humerus. *The Journal of Bone and Joint Surgery* 2003;85:611-617. doi: 10.1302/0301-620x.85b4.12843
40. Utz CJ, Bauer TW and Iannotti JP. Glenoid component loosening due to deficient subscapularis: a case study of eccentric loading. *Journal of Shoulder and Elbow Surgery* 2011;20:e16-e21. doi: 10.1016/j.jse.2011.03.024
41. Van den Berghe GR, Nguyen B, Patil S, D'Lima DD, Mahar A, Pedowitz R and Hoenecke HR. A biomechanical evaluation of three surgical techniques for subscapularis repair. *J Shoulder Elbow Surg* 2008;17:156-61. doi: 10.1016/j.jse.2007.04.016
42. Van Thiel GS, Wang VM, Wang FC, Nho SJ, Piasecki DP, Bach BR, Jr. and Romeo AA. Biomechanical similarities among subscapularis repairs after shoulder arthroplasty. *J Shoulder Elbow Surg* 2010;19:657-63. doi: 10.1016/j.jse.2010.01.014